

FD-503 (FORM 6-62)

N66 33180

(ACCESSION NUMBER)

81

(PAGES)

CR-63431

(NASA CR OR TMX OR AD NUMBER)

(THRU)

1

(CODE)

33

(CATEGORY)

PROJECT FILE

02

04268-9-P

THE UNIVERSITY OF MICHIGAN

COLLEGE OF ENGINEERING

DEPARTMENT OF MECHANICAL ENGINEERING
HEAT TRANSFER AND THERMODYNAMICS LABORATORY

Progress Report No. 7

(For the Period November, 1963 - November, 1964)

Pressurization of Liquid Oxygen Containers

J. A. CLARK
H. MERTE, JR.
W. J. YANG
E. LEWIS
H. BARAKAT
B. BAILEY
N. TOKUDA

GPO PRICE \$ _____

CFSTI PRICE(S) \$ _____

Hard copy (HC) \$3.00

Microfiche (MF) 1.75

853 July 65

Under contract with:

National Aeronautics and Space Administration
George C. Marshall Space Flight Center
Contract No. NAS-8-825
Huntsville, Alabama

Administered through:

January 1965

OFFICE OF RESEARCH ADMINISTRATION • ANN ARBOR

Eq 29577

THE UNIVERSITY OF MICHIGAN
COLLEGE OF ENGINEERING
Department of Mechanical Engineering
Heat Transfer and Thermodynamics Laboratory

Progress Report No. 7
(For the Period November, 1963 - November, 1964)

PRESSURIZATION OF LIQUID OXYGEN CONTAINERS

J. A. Clark
H. Merte, Jr.
W. J. Yang
E. Lewis
H. Barakat
B. Bailey
N. Tokuda

ORA Project 04268

under contract with:

NATIONAL AERONAUTICS AND SPACE ADMINISTRATION
GEORGE C. MARSHALL SPACE FLIGHT CENTER
CONTRACT NO. NAS-8-825
HUNTSVILLE, ALABAMA

administered through:

OFFICE OF RESEARCH ADMINISTRATION

ANN ARBOR

January 1965




TABLE OF CONTENTS

	Page
LIST OF ILLUSTRATIONS	v
NOMENCLATURE	vii
ABSTRACTS	xi
I. PRESSURIZATION, STRATIFICATION, AND INTERFACIAL PHENOMENA	1
II. BOILING OF A CRYOGENIC FLUID UNDER REDUCED GRAVITY	3
A. General	3
B. Heat Transfer Surface Geometry	4
1. Spheres	4
2. Flat Surface (disc)	4
C. Variables Studied	6
1. Configuration and Orientation	6
2. Boiling Regime	6
3. Subcooling	6
4. Pressure	7
5. Gravity	8
D. Test Procedures and Results	9
1. Flat Surface (disc)	9
E. Modifications to Facilities for the Use of Liquid Hydrogen	11
F. Future Efforts	13
1. Liquid Nitrogen	13
2. Liquid Hydrogen	13
III. INCIPIENT BOILING OF LIQUID HYDROGEN	15
IV. BOILING OF CRYOGENIC LIQUID UNDER HIGH GRAVITY	17
V. INJECTION COOLING	19
A. Introduction	19
B. Model and Analysis	19
1. Temperature Distribution	22
2. Solution for the Bubble Growth Rate	24
C. Results and Discussion	31
1. Temperature Distribution	31
2. Bubble Growth or Collapse	32
D. Conclusions	32

TABLE OF CONTENTS

	Page
VI. TRANSIENT, LAMINAR FREE CONVECTION HEAT TRANSFER IN TWO-DIMENSIONAL CONTAINERS	35
A. Analytical Work	35
B. Experimental Work	40
C. Analytical Study of the Velocity Transients During the Pressurized Discharge	40
REFERENCES	43

LIST OF ILLUSTRATIONS

Table	Page
I. Summary of Tests Conducted with Fractional Gravity in This Period	8

Figure

1. Accelerometer measurements on inner package.
2. Computer output plot—boiling of liquid nitrogen under free fall.
3. Modified disc for transient heat transfer measurement.
4. Pressurized test vessel.
5. Boiling data with disc (vertical), $P = 1$ atm, saturated.
6. Boiling data with disc (vertical), $P = 3$ atm, saturated.
7. Boiling data with disc (vertical), $P = 3$ atm, subcooled.
8. Boiling data with disc (vertical), $P = 5$ atm, saturated.
9. Boiling data with disc (vertical), $P = 5$ atm, subcooled.
10. Boiling data with disc (horizontal up), $P = 1$ atm, saturated.
11. Boiling data with disc (horizontal up), $P = 5$ atm, saturated.
12. Boiling data with disc (horizontal up), $P = 5$ atm, subcooled.
13. Boiling data with disc (horizontal down), $P = 1$ atm, saturated.
14. Boiling data with disc (horizontal down), $P = 5$ atm, saturated.
15. Boiling data with disc (horizontal down), $P = 5$ atm, subcooled.
16. Zero-gravity liquid hydrogen research facility.
17. Liquid hydrogen zero-gravity test package assembly.

LIST OF ILLUSTRATIONS (Concluded)

Figure

18. Flow about a spherical bubble.
19. Distribution of first-order temperature functions.
20. Distribution of first- and second-order temperature functions.
21. Distribution of first- and second-order temperature functions.
22. Bubble growth. Quasi-steady case.
23. Bubble growth. Quasi-steady case.
24. Bubble growth for large acceleration case.
25. Coordinate system for cylindrical tank.
26. Transient flow pattern for cylindrical tank—small time.
27. Transient flow pattern for cylindrical tank—large time.

NOMENCLATURE
(Part V)

- C : constant in Eq. (2) = $\frac{16}{3} \frac{\rho_L - \rho_g}{\rho_L} \frac{g}{C'v}$ [sec⁻¹·cm⁻¹]
- C' : non-dimensional constant = 41 by Levich (4)
- C_p : Drag coefficient. non-dimensional
- D_{ij}ⁿ : Function showing the nth power effect of (τ_i, ξ_j)
- F_{ij}ⁿ : Function showing the nth power effect of (τ_i, τ_j)
- f_{ij}ⁿ : Function showing the nth power effect of (ξ_i, ξ_j)
- g : gravitational acceleration [cm/sec²]
- k : thermal conductivity [cal/sec °C cm]
- K : constant in Eq. (3) given by Miyagi (5) [sec⁻¹]
- L : latent heat [Kcal/kg]
- p : pressure [Kg/cm²]
- Pe : Pecklet No = $\frac{2U_0R_0}{\alpha}$
- R : Bubble radius [cm]
- r : non-dimensional radius = R/R₀ or radial co-ordinate in spherical co-ordinate system
- T : Temperature [°C]
- t : time [sec]
- U : velocity [cm/sec]
- U_∞ : translatory velocity of the bubble [cm/sec]
- u : non-dimensional velocity = U/U₀
- V : volume of the bubble [cm³]

NOMENCLATURE (Continued)

X : co-ordinate

Greek Letters

α : thermal diffusivity = $\rho C_p/k$ [cm^2/sec]

β : angular co-ordinate

γ : non-dimensional constant to be given as $\gamma = \frac{2 \times 0.0504}{R_o} \frac{g}{U_o^2} = 0.85 \frac{1}{Re \times R_o^2}$ (must be evaluated c-g-s unit by Miyagi (5))

δ : non-dimensional quantity = $\frac{L}{C_p(T_\infty - T_s)}$ or boundary layer thickness

ϵ_i : similarity variables with respect to velocity change

τ_i : similarity variables with respect to boundary movement

τ : non-dimensional time = $\frac{V_o}{R_o} t$ or stress [kg/cm^2]

η : similarity variable = $(r-R) \sqrt{\frac{U}{dX}}$ or $(r-R) \sqrt{\frac{\dot{U}}{\alpha U}}$

ν : viscosity [cm^2/sec]

ρ : density [Kg/cm^3]

σ : surface tension [dyn/cm]

θ : non-dimensional temperature = $\frac{T_\infty - T}{T_\infty - T_s}$

μ : viscosity [$\text{Kg}/\text{sec} \cdot \text{cm}$]

Subscripts

o : steady initial state.

s : saturation

∞ : condition at ∞

n : normal component

NOMENCLATURE (Continued)

t : tangential component

(Part VI)

a : radius of the container

b : the initial height of the liquid

C_p : constant pressure specific heat, BTU/lbm°F

Gr : Grashof number = $g\beta(T_s - T_o)a^3/\nu^2$

g : the acceleration of gravity, ft/sec²

k : thermal conductivity, BTU/hr ft°F

p : pressure

Pr : Prandtl number = ν/α

Ra : Rayleigh number, (GrPr)

$(q/A)_w$: heat flux at the walls of the tank per unit area, BTU/hr-ft²

T : temp R

t : time, sec.

u : x-component of the velocity, ft/sec

v : r-component of the velocity, ft/sec

U : dimensionless x-component of the velocity

V : dimensionless r-component of the velocity

w : flow rate

x : axial distance, ft

X : dimensionless x

NOMENCLATURE (Concluded)

- r : radial distance measured from the center of the tank, ft
- R : dimensionless r
- w : $w = \frac{1}{R^2} \left(\frac{a^2}{b^2} \frac{\partial^2 \psi}{\partial x^2} + \frac{\partial^2 \psi}{\partial R^2} - \frac{1}{R} \frac{\partial \psi}{\partial R} \right)$
- α : thermal diffusivity, ft²/sec
- β : coefficient of thermal expansion.
- ρ : density, lbm/ft³
- μ : viscosity, lbm/ft-sec
- ν : kinematic viscosity, ft²/sec
- τ : dimensionless time
- Θ : dimensionless temperature
- ψ : stream function

Subscripts

- s : saturation or liquid surface
- i,j : denotes position in the space grid.
- o : denotes initial conditions
- w : wall

Superscript

- n : denotes the time level

ABSTRACTS

- I. A comprehensive summary of the subject of pressurization, stratification, and interfacial phenomena has been completed and is referenced.
- II. Descriptions of the test vessel and test procedures followed in obtaining subcooled nucleate boiling data of liquid nitrogen under fractional gravity and free-fall conditions are given. Data are presented in the film boiling region from a disc (flat surface) with a vertical orientation, horizontal facing downward, and horizontal facing upward. The effects of pressure, subcooling, gravity, and orientation are noted. In addition, descriptions are given of modifications to the test facility for use with liquid hydrogen.
- III. Design work will be initiated on a test facility to determine with precision the incipient boiling conditions with liquid hydrogen.
- IV. The design of a test vessel for obtaining measurements of pool boiling of liquid nitrogen under high gravity fields, up to $a/g = 100$, will be initiated.
- V. A power-series solution is obtained for the temperature field in the liquid in which a spherical bubble is growing as a result of a step change in the boundary movement and/or translatory velocity of the bubble. Bubble growth rates are obtained for the quasi-steady small acceleration and large acceleration cases.
- VI. The two-dimensional laminar, transient free convection heat and mass transfer in cylindrical containers is analyzed using the numerical method of Ref. 7. The numerical method is briefly described and the results obtained for the flow pattern at two different time levels are given.

I. PRESSURIZATION, STRATIFICATION, AND INTERFACIAL PHENOMENA

A summary report titled "Pressurization, Stratification, and Interfacial Phenomena," by J. A. Clark was written for the 1964 Cryogenic Engineering Conference as paper A-6. This report includes a summary of The University of Michigan work on this subject to date as well as summarizing that of several other institutions.

Copies of this report were sent to the contract monitors at the George C. Marshall Space Flight Center in August 1964. Owing to its length it will not be reproduced here. Copies may be obtained by writing to the principal author of this progress report. It also will be published in the forthcoming volume Advances in Cryogenic Engineering, Vol. 10, K. D. Timmerhouse, Editor, Plenum Press.

II. BOILING OF A CRYOGENIC FLUID UNDER REDUCED GRAVITY

A. GENERAL

During the past reporting period a large number of tests were conducted of boiling heat transfer with liquid nitrogen under free fall and fractional gravity conditions.

The test package described in Fig. 8 of Ref. 1 was used for all these tests and performed satisfactorily for both free fall ($a/g \approx 0$) and fractional gravity. For "0" g tests the inner test package is released simultaneously with the outer package, which serves as a shield and permits relative internal motion. Figure 1 is a recording of the output of the 0-1 g Kistler Model 303 Accelerometer, attached to the inner test package during free-fall tests. These particular tests were conducted to determine if the connecting thermocouple wires between the inner and outer packages exerted any detectable forces on the free floating inner package. It is noted that no effect is present. Although an initial oscillation is present on release, due to the dynamic characteristics of the cushioned accelerometer mounting, these are rapidly damped out and the maximum subsequent change in effective gravity taking place during the free-fall period is less than 0.005 g. This is to be compared with Fig. 3 of Ref. 1 which indicates a maximum variation of ± 0.01 g with the original single test package. A number of other tests with the accelerometer on the inner package have shown that the maximum level of effective gravity may well be less than 0.001 g, on the order of the resolution of the recorder.

With the use of the double package concept for the achievement of $a/g \approx 0$, problems arose due to high impact shocks occurring on the inner package when contact was made with the outer package at the conclusion of a drop. Deformation of the supports of the test objects within the inner package occurred, sometimes breaking the connecting thermocouple wires. Lining the bottom of the outer package with foam rubber was not satisfactory as the spillage of liquid nitrogen and the low temperature environment around the inner package caused it to harden with time. The difficulty was solved temporarily by providing stiffer supports for the test objects, but future tests, particularly with a test package used to contain liquid hydrogen, will make the presence of large impact shocks undesirable. To provide a quantitative means for determining the magnitude and duration of the impact shocks, and thereby aid in reducing them in future tests, a Kistler Model 808A quartz crystal high level accelerometer ($10,000 g_{\max}$) has been procured. Tests have indicated that momentary shocks on the order of 300-400 g's exist on the inner package.

PRECEDING PAGE BLANK NOT FILMED.

B. HEAT TRANSFER SURFACE GEOMETRY

1. Spheres

Data have been reported previously in all regions of boiling with spheres of 1, 1/2, and 1/4 in. diameters at $a/g = 1$ and reduced gravities with saturated liquid nitrogen at atmospheric pressure. No differences in behavior were noted between the 1 and 1/2 in. diameter spheres, whereas a distinct change occurred in the film boiling characteristics with the 1/4 in. diameter sphere, as might be noted in Figs. 12-14 of Ref. 1. Additional data have been obtained with the 1 and 1/4 in. diameter spheres, with saturated and sub-cooled liquid nitrogen, and at pressures up to 5 atmospheres.

For the 1 in. diameter sphere, the transient temperature measurements are made at the center and near the surface, and a digital computer program described in previous reports is used in the data reduction process for the sake of convenience and to improve the accuracy in the nucleate boiling region. At times oscillations in output results have occurred as a consequence of the use of unsmoothed input data in conjunction with the computational procedures used. The program was modified to provide a smoothing of the temperature-time derivatives with a least-mean-square fit procedure. Also, a direct computer-plotted output procedure was incorporated to permit immediate detection of errors. An example of this type of output is shown in Fig. 2. Superimposed on the plot for reference are the representative data at $a/g = 1$.

Due to size limitations a single thermocouple is inserted in the 1/4 in. diameter sphere, and the sphere treated as a lumped system within an acceptable approximation. The digital computer program is still used to determine time-rates of temperature change.

2. Flat Surface (disc)

The sphere is a special surface in that in a directional force field it includes surfaces having all possible orientation. Under long term zero-gravity conditions the orientation of the heater surface, of course, should not affect the results. With fractional gravity conditions, however, as well as the short term zero-gravity present with the drop tower technique used here, it might be anticipated that the orientation of a flat surface would influence the boiling heat transfer. In the case of short time zero-gravity this could represent the effect of residual liquid motion imparted prior to release of the test vessel.

Measurements of boiling heat transfer characteristics have been made with a flat surface with various orientations. With the short test periods available it was desired to continue the use of the transient technique. The disc

used initially was constructed as indicated in Ref. 2, which also describes the design principles followed. Several narrow concentric grooves were machined on the inner sides of the disc in order to form the guard heaters necessary for the computation of heat flux at the surface from the transient temperatures measured in the central portion. To perform the machining of these grooves it was found necessary to use "leaded" copper, a free machining copper containing 1% lead. Accurate computations of heat flux in the boiling regions of high heat flux such as nucleate and transitional required that temperature differentials be measured within the central region of the disc, and for the rapid response required it was necessary to solder the thermocouples at the bottom of the drilled holes, using the parent metal as the intermediate connection between junctions. Physically unreasonable values of temperature differentials were obtained, and these have been attributed to inhomogeneities in the leaded copper, giving rise to EMF's which could not be related to temperature differences.

It was necessary to make a new disc using electrolytic copper. Since the narrow concentric grooves necessary to avoid edge effects could no longer be machined in the soft copper, a redesign of the disc was made. The central test portion of the disc was made square, rather than circular, so that screw-slotting cutters operating at high speed could be used to machine the slots. The slots were terminated before emerging from the periphery of the disc. Figure 3 shows a sketch of the new disc. An additional set of slots is present to further isolate the central test portion from edge effects, requiring a somewhat larger disc.

As in the prior design, two such discs are placed back-to-back, with a 1/16 in. gap on the central plane to provide as close to an adiabatic surface as possible. The two halves are held together with screws on the 1/4 in. wide peripheral mating surface, which is sealed with a rubber-type cement.

Holes .040 in. in diameter are drilled outward from the central plane in one of the discs for purposes of soldering thermocouple junctions at the bottom. Figure 3 shows the location of these and the respective recorder connections. ΔT_s measures the temperature .030 in. from the heat transfer surface with respect to the ice point; ΔT_1 is the temperature difference between this same point and the adiabatic centerline; ΔT_2 is the temperature difference between the adiabatic centerline and a point midway to the heat transfer surface; and ΔT_3 is the temperature difference between corresponding points in the central test region and the first guard ring, serving as an indication of the effectiveness of the thermal guard rings.

With the additional information on transient temperature distributions within the slab, more accurate values of heat flux at the heat transfer surface can be computed in the regions of high heat flux. Data obtained to date with the disc have been primarily in the film boiling region where a lumped system analysis is satisfactory, the Biot Number being on the order of 0.005.

A digital computer program has recently been completed to permit data reduction in the transition, maximum heat flux, and nucleate boiling regions for the distributed system. This will be described in the next report with representative results.

The orientations of the flat surface of major interest are vertical, horizontal facing upward, and horizontal facing downward, the directions being indicated with respect to the normal gravity field. The direction and magnitude of bulk liquid motion, along with the facility of vapor removal from the vicinity of the heat transfer surface may reasonably be expected to differ with these orientations, resulting in changes in heat transfer characteristics.

C. VARIABLES STUDIED

For convenience the range of variables covered in the test data to be presented are listed. Because of the number of variables, coverage of all possible combinations was not practical, and judicious selection became necessary in an attempt to disclose significant trends.

1. Configuration and Orientation

- a. Spheres.—1 and 1/4 in. diameter, discussed in Section B-1 above.
- b. Flat Surfaces.—3 in. diameter disc, vertical, horizontal facing up, horizontal facing down, discussed in Section B-2 above.

2. Boiling Regime

Using liquid nitrogen, data are presented for all regions of boiling from film boiling with ΔT 's of 300°F through the transition, maximum heat flux, and nucleate boiling regions. For tests with subcooled liquid nitrogen, some data are available for non-boiling convection as well. A large amount of the test data presented here applies to the film boiling region, but again because of the large number of variables only a sufficient number were conducted to disclose a meaningful trend. All other variables being held constant, from two to four tests were conducted with various values of ΔT in the film boiling region for each test condition.

3. Subcooling

The results of tests presented heretofore (e.g., Ref. 1) dealt with the influence of standard, fractional, and short time zero-gravity on the various boiling regimes with a saturated cryogenic liquid, nitrogen. As an extension of these results, it was desired to determine the additional effects

that subcooling of the bulk liquid would have on the pool boiling process with reduced gravity. The method adopted as most convenient to achieving subcooling was rapid pressurization of the test vessel with helium. Nominal pressures of 3 and 5 atmospheres were selected, giving initial subcoolings of 19.3°F and 30.3°F, respectively. With the transient technique employed to obtain the heat transfer data, immersing the heated test object in the bulk liquid, it was not possible to hold the subcooling constant to the degree that might have been desired. The extent to which the bulk liquid heated as the test object was cooled depends upon the relation between the total heat capacity of the bulk subcooled liquid and the heat capacity of the test object, along with the particular portion of the boiling curve at which the data are desired.

To date the test objects have been immersed in the liquid nitrogen while near room temperature and permitted to cool down to the region of interest. With the 1/4 in. diameter sphere the change in subcooling upon cooling down to the nucleate boiling region is negligible, and is small with the 1 in. diameter sphere. With the disc, however, appreciable heating of the subcooled liquid does take place because of its large heat capacity. To circumvent the variation in subcooling, provision may be made to precool the test object to near the desired range prior to immersing it in the subcooled liquid. As will be pointed out, however, it has been found that subcooling greater than some minimum value, as yet indetermined, appears to have no influence on the film boiling process.

A split cover was installed on the outer vessel for pressurization, as shown on Fig. 4. On one half of the cover were installed the pressurizing valve, a pressure relief valve, a strain gage pressure transducer for recording purposes, and the necessary electrical connections into the outer vessel. The other half furnished access between tests for heating the test object and filling the inner vessel. The test object is attached to a hinged arm and inserted into the liquid nitrogen at the desired time remotely by activating a solenoid.

The temperature of the bulk liquid is monitored continuously with a thermocouple located approximately 1 in. from the test object in the same horizontal plane. With the intense agitation induced by the boiling process it is not felt that appreciable stratification takes place. From the saturation temperature corresponding to the pressure the degree of subcooling is computed.

4. Pressure

As pointed out in the previous section, the range of pressures covered in these tests are 1, 3, and 5 atmospheres, nominal. With the technique of pressurization with an inert gas used to achieve subcooling, two variables are introduced, pressure and subcooling, each of which may and indeed does influence the boiling process. To determine the effect of subcooling alone,

the effect of pressure must also be determined. To this end, data were obtained with the various test objects for saturated liquid nitrogen at 3 and 5 atmospheres pressure. The vessel was pressurized with nitrogen gas, and ambient heating brought the liquid nitrogen to its saturation temperature prior to inserting the test object.

The pressure is regulated manually while the test vessel is at rest at standard gravity. The off-gasing associated with boiling from the test object tends to increase the pressure if no venting takes place, as is necessary during the free-fall or fractional gravity test drop period. However, the outer vessel has sufficient volume that during the short drop time the pressure increase may be neglected.

5. Gravity

Prior data have been reported for body forces corresponding to the following relative accelerations: $a/g = 1, 0.60, 0.33, 0.20$, and free-fall ($a/g < .001$). Again, to keep the total number of tests conducted reasonable with the variables to be considered, the tests reported here were conducted for the most part at: $a/g = 1, 0.20$, and free-fall ($a/g < 0.001$). It was felt that a single fractional gravity would furnish the desired indications.

The number of tests conducted during the past reporting period are summarized below in Table I in the categories of geometry and gravity. Within each condition shown are contained the variables of pressure and subcooling, some to a greater or lesser extent.

TABLE I
SUMMARY OF TESTS CONDUCTED
WITH FRACTIONAL GRAVITY IN THIS PERIOD

Test Object	$a/g = 1$	$a/g = 0.2$	Free-Fall $a/g < .003$	Total
1/4 in. sphere	5	22	5	32
1 in. sphere	29	15	19	63
Disc-V	9	15	28	52
Disc-HU	3	9	9	21
Disc-HD	3	9	6	18
Totals	49	70	67	186

D. TEST PROCEDURES AND RESULTS

Prior to each test the outer vessel was opened and the test object brought up to room temperature. For zero-gravity tests the inner test vessel was suspended from the friction release pawl and filled with liquid nitrogen. For fractional gravity tests the inner vessel rested on the bottom of the outer vessel. The test object was then placed in position for subsequent immersion in the liquid nitrogen by a solenoid release, and the outer vessel closed. The Sanborn recorder is then calibrated.

For obtaining subcooled data, the vessel is pressurized, the test object inserted, and the outer vessel released at the desired point on the boiling curve. For data with saturated liquid under pressurization, the test object is not immersed until the liquid has reached its saturation temperature, and then the outer vessel is released.

The results reduced to completion to date are presented below for the disc, subdivided first according to orientation, and then pressure, subcooling and gravity. Results have been obtained for the 1 in. and 1/4 in. diameter spheres, but the data reduction are not yet complete. These will be reported in the next period.

1. Flat Surface (disc)

a. Vertical Orientation.—

i. P = 1 Atmosphere, Saturated.—Figure 5 indicates data obtained with the disc in a vertical position, in the film boiling region, with saturated liquid nitrogen at atmospheric pressure, for standard gravity ($a/g = 1$), for fractional gravity ($a/g = 0.2$), and free-fall ($0.001 \leq a/g \leq 0.003$). It is noted that for a given ΔT , the heat transfer rates are considerably higher than that obtained with the 1 in. diameter sphere. The heat transfer rates with free-fall do not appear to be considerably less than that for $a/g = 0.2$. This may be a consequence of the large liquid motion induced by virtue of the large mass and size of the disc.

Several additional tests are planned for $a/g = 0.2$ at the lower levels of ΔT in the film boiling region and in the nucleate boiling region.

ii. P = 3 Atmosphere, Saturated.—Figure 6 presents data similar to that in Fig. 5 except for a nominal pressure of 3 atmospheres. At $a/g = 1$, the rate of heat transfer is greater than at one atmosphere pressure. Again, several additional data points are to be obtained at the lower levels of ΔT in the film boiling range for $a/g = 0.2$ and free-fall.

iii. P = 3 Atmosphere, Subcooled.—Figure 7 shows data for the vertical disc with various degrees of subcooling. Run 65B covered the entire

film boiling range, and the subcooling decreased from an initial value of 12°F at the highest ΔT to saturated liquid at the lowest ΔT due to the heating of the liquid by the disc. Thus, data near the low values of ΔT should be considered as saturated data at this pressure. By comparing Figs. 6 and 7, it is noted that at the high values of ΔT , with large subcooling, the effect of subcooling is to increase the heat flux with film boiling at $a/g = 1$. Several additional data points are necessary at $a/g = 0.2$ and free-fall to make conclusive statements for these conditions.

iv. P = 5 Atmosphere, Saturated.—Figure 8 presents data obtained with saturated liquid nitrogen at 5 atmosphere pressure. On comparison with Fig. 6, a further increase in heat flux with pressure is observed. The change in heat flux with reduction in a/g , however, is less than at the lower pressures. This might be anticipated since the buoyant forces decrease with increasing pressure due to density effects.

v. P = 5 Atmosphere, Subcooled.—In Fig. 9, data corresponding to Fig. 8 are presented, except that the liquid nitrogen is subcooled. Again, the differences between saturated and subcooled data are more pronounced at the higher values of ΔT , where subcooling is the largest.

b. Horizontal Orientation (Test Surface Up).—Figures 10-12 indicate data with the flat heating surface facing upward, for $P = 1$ atm.—saturated, $P = 5$ atm.—saturated, and $P = 5$ atm.—subcooled, respectively. In determining the influence of orientation, a single pressure for the subcooled case was deemed sufficient. For $P = 1$ atm.—saturated, comparison can be made between Figs. 5 and 10. At $a/g = 1$, no difference exists in behavior of film boiling, whereas with fractional gravity and free-fall, the heat flux decreases to a greater extent with the vertical orientation than the horizontal-up position. This behavior would seem to exclude the possibility that the fluid motion was a significant factor, since the fluid motion is expected to be greater for the vertical case than the horizontal one. Similar effects occur at $P = 5$ atm.—saturated, noted by comparing Figs. 6 and 11, and at $P = 5$ atm.—subcooled, by comparing Figs. 7 and 12. In test Run 71L of Fig. 12, the data appear unusually high. Similar behavior occurred with a subsequent re-run, to be reported later. Also, in Fig. 12, the instantaneous values of bulk subcooling are listed along the data points for Run 69F.

c. Horizontal Orientation (Test Surface Down).—Figures 13-15 indicate data obtained with the flat heating surface facing downward, for $P = 1$ atm.—saturated, $P = 5$ atm.—saturated, and $P = 5$ atm.—subcooled, respectively.

In all cases, the changes in heat flux resulting from decrease in gravity are small, as might be anticipated. With this orientation the body forces tend to keep the vapor in the vicinity of the heating surface. With Run 70B on Fig. 14, the pressure did not remain constant due to experimental difficulties, and the instantaneous values are tabulated along the data points.

Comparing Figs. 10 and 13 for $P = 1$ atm-saturated, Figs. 11 and 14 for $P = 5$ atm-saturated, and Figs. 12 and 15 for $P = 5$ atm-subcooled, it is observed that virtually no differences in behavior exist between the horizontal up and the horizontal down orientations at $a/g = 1$, and the differences at reduced gravity are very small. When the remaining data available has been reduced, these plots will be combined to show more graphically the individual effects of pressure, subcooling, and orientation.

E. MODIFICATIONS TO FACILITIES FOR THE USE OF LIQUID HYDROGEN

Planning and engineering design work has been completed to provide the facilities for obtaining boiling heat transfer data to liquid hydrogen under standard gravity, fractional gravity and short time zero-gravity, with free-fall. Fire and safety regulations prohibit the storage of liquid hydrogen containers within an enclosed space. This dictated the necessity of using the roof of the building as the upper terminal of the drop tower, as the liquid hydrogen storage dewar could be left in the open, with transfer of liquid hydrogen to the test vessel taking place through appropriate vacuum insulated lines in an atmospheric vented space. Since openings in the roof large enough to provide necessary communication between the present instrumentation area and the upper working area could not be made, the shelter area on the roof was enlarged to permit the location of all instrumentation and operations at this level. Preliminary cost estimates for this construction have been obtained and exceed considerably that originally estimated. This is a consequence of the required roof-installation, additional safety and venting provisions and structural engineering and architectural demands of The University of Michigan. Additional and final cost estimates are presently being obtained.

It is planned that the boiling heat transfer data will be obtained using the same transient technique as with liquid nitrogen. To prevent contact of liquid hydrogen with air, with the resultant contamination due to solidification of the oxygen and nitrogen, a closed vessel will be constructed. Since the transient technique results in net generation of vapor, venting of hydrogen vapor will be necessary by means of a pressure relief valve during the various phases of the test operation. This includes the period while the test vessel is at the top of the drop tower, during free-fall, and at the end of the drop period with the vessel at the bottom of the tower. To contain the vented hydrogen the entire drop area will be enclosed in an aluminum duct approximately four feet square, terminating at the lower end in a chamber housing the buffer, and at the upper end in a chamber isolated from the instrumentation and working area. The arrangements of this facility are shown in Fig. 16.

In the roof of the shaft-head chamber is located an explosion-proof exhaust fan capable of providing approximately 120 air changes per hour in the working space where hydrogen might be expected. The shaft-head chamber is

isolated from the operating area by an "air-lock" room to prevent any possibility of hydrogen getting into the working area. A 4-point hydrogen detector will be installed to sample the air at various locations in the test area, and will sound an alarm and start the exhaust fan automatically should a hazardous accumulation exist. The outer wall of the shaft-head chamber consists of a blowout type panel and door.

The lower part of the buffer chamber has inward opening louvers to provide a source of air for the exhaust fan, and both the buffer and shaft-head chambers will have 8 CO₂ cylinders for flooding the test chamber should the need arise. The normal operating procedure will be such that the ventilating fan will be operating at all times any hydrogen is being handled or used except for the short period, approximately 2 sec, that the actual drop takes. The fan will be shut-off during this period to avoid excessive air drag.

Because of interference of the buffer chamber with a gasometer at the lower level, and cooling tower supports at the roof level of the present location, the drop tower is being relocated to a floor hatch opening 24 feet away in the Fluids Engineering Laboratory. This will bring the research area closer to the stairway and freight elevator leading to the roof level.

Figure 17 shows a cross sectional view of the proposed test vessel to be used with liquid hydrogen. It consists essentially of a superinsulated cryostat contained within a double-wall vessel. The primary heat leakage to the liquid hydrogen will be via the tube serving as the opening, and is minimized by necking the section down and providing a liquid nitrogen bath around the cover. This bath also eliminates the heat leakage from the environment via the main support rods.

Liquid hydrogen is charged into the cryostat through a vacuum insulated line passing through the liquid nitrogen bath. Also connected to the cryostat at the main flanged opening are two vent tubes, one for a pressure relief valve, the other for a rupture disc and pressure measurement, a high and low liquid level detector, and two bulk liquid thermocouples.

Associated with the liquid nitrogen bath are a fill tube and a liquid level detector. Venting of the nitrogen vapor will take place through a pressure regulating valve in the cover. With suitable initial purging of the vapor space around the cryostat, this arrangement will provide an inert atmosphere completely surrounding the cryostat, an additional safety factor should the cryostat rupture.

The test object, initially a sphere, is inserted into the liquid hydrogen by means of a long hollow SS rod extending through the heating chamber cover and the outer vessel cover, sealed with several sets of Teflon "O" rings. Since temperatures in these regions will be above liquid nitrogen temperatures no difficulties in sealing are anticipated. Thermocouple connections to the sphere will be made through the hollow rod, with the pressure seal at the room temperature end.

In order to make a number of test runs with a single charge of liquid hydrogen, it is necessary that the test object be heated after a particular test without removal from the vessel. With the test object within the heating chamber, heating will take place by radiation from an electrical tubular heating element formed in the shape of a cylinder. Electrical termination of the heater element will take place external to the test vessel. Radiation shields below the test object will isolate the radiant heaters from the liquid hydrogen, and tubular coils surrounding the heaters will reduce heat transfer to the liquid nitrogen bath during the heating process and cool the chamber down once heating has stopped by circulating liquid nitrogen through the coils. A thermocouple will be attached to the radiant heater coil to monitor its temperature, and another thermocouple will measure the heating chamber vapor temperature.

Surrounding the double-wall outer vessel is an air-resistance shield, for use in free-fall tests to obtain as near to zero-gravity as possible. This shield is released simultaneously with the test package by means of a solenoid actuated release yoke and ring as shown in the upper portion of Fig. 17.

F. FUTURE EFFORTS

1. Liquid Nitrogen

The majority of tests concerned with subcooled pool boiling have been completed and are being processed. These include additional data for the flat surface and for the sphere, and will be reported in the next reporting periods as they become available.

2. Liquid Hydrogen

Design of the test vessel for the use of liquid hydrogen will be continued, as will the design effort associated with modification to the drop-tower facility.

III. INCIPIENT BOILING OF LIQUID HYDROGEN

Design work will be initiated during the next reporting period on a test facility to determine with precision the incipient boiling conditions with liquid hydrogen. This will include simultaneous steady state thermal measurements and visual observations.

PRECEDING PAGE BLANK NOT FILMED.

IV. BOILING OF A CRYOGENIC LIQUID UNDER HIGH GRAVITY

The design of a test vessel for obtaining measurements of pool boiling of a cryogenic liquid, initially liquid nitrogen, under high gravity fields, up to $a/g = 100$, will be initiated. The availability of a large centrifuge in the laboratory will permit the use of a vessel of sufficient size to obtain data with subcooled liquid nitrogen and with pressures higher than atmospheric. Also, the transient technique using both a flat disc and a sphere can be incorporated so that data over the entire boiling range can be obtained, including nucleate, maximum heat flux, transition and film boiling.

PRECEDING PAGE BLANK NOT FILMED.

Page intentionally left blank

V. INJECTION COOLING

A. INTRODUCTION

Bubble growth or collapse in the injection cooling has been analytically and experimentally investigated in Ref. 9. This section is to report a preliminary study on the growth or collapse of a spherical bubble with translatory motion. In order to understand the basic mechanism involved, a simple model is formulated in which the bubble growth or collapse is governed only by its translatory motion and energy diffusion in the liquid. It is anticipated that in the next period, the model will be modified to include the simultaneous diffusion of mass. By means of transferring the reference frame from liquid to the moving bubble, the problem becomes that of a uniform flow about a spherical bubble. This transformation of the coordinate systems has an advantage in the formulation of the problem without changing the physics.

B. MODEL AND ANALYSIS

The physical system analyzed is shown in Fig. 18. It consists of a uniform flow about a spherical bubble with radius R . If the bubble is sufficiently small in size (0.3~0.5 cm diameter), it maintains a spherical form. Under the isothermal condition throughout the system, Chao³ and Leuich⁴ have obtained a relationship between the drag coefficient and flow condition around the bubble as

$$C_D = C'/Re \quad (1)$$

for quasi-steady state. This indicates that if the change in the flow velocity is sufficiently small, compared with the velocity itself, then the translatory motion of the bubble is directly proportional to the square of the bubble radius or

$$U_\infty = CR^2 \quad (2)$$

On the contrary, if the change in the flow velocity is very large compared with the velocity, Miyagi⁵ in his experimental study of an air bubble rising in water, has proposed

$$U_\infty = U_0 \left(1 - \frac{2}{1 + e^{kt}} \right) \quad (3)$$

for the initial period of the bubble's translatory motion. In this analysis these two velocity changes are imposed on the system as a disturbance which causes the bubble to either grow or collapse. Beside the translatory velocity, a change in the liquid temperature at a distance from the bubble moving at a constant velocity may be regarded as another disturbance. The most general case is the one in which these two disturbances are simultaneously imposed on the system. It is the purpose of this analysis to investigate the time-history of bubble size under such circumstances.

The following assumptions are imposed on the analysis: (a) The flow around the bubble is ideal and equal to the translatory velocity of the bubble U_∞ . (b) The vapor temperature inside the bubble is uniform (or lumped) and equal to the surface temperature of the bubble. The first assumption needs some justification: Since the tangential and normal components of the vapor velocity inside the bubble and the velocity of the liquid outside the bubble have to be equal one writes

$$U'_t = U''_t \quad (4)$$

and

$$U'_n = U''_n = \dot{R}(t) \quad (5)$$

Furthermore, the force balance in the radial and tangential directions requires

$$F'_n = F''_n \quad \text{or} \quad \tau'_{nn} + \tau'_\sigma = \tau''_{nn} \quad (6)$$

$$F'_t = F''_t \quad \text{or} \quad \tau'_{tt} + \tau'_t = \tau''_{tt} \quad (7)$$

where

$$\tau'_\sigma = \sigma \frac{\partial^2 \xi}{\partial x^2} \quad \text{and} \quad \tau'_t = \sigma \frac{\partial^2 \xi}{\partial y^2} \quad (8)$$

Equations (6) and (7) may be rewritten as

$$P'' - P' = \sigma \frac{\partial^2 \xi}{\partial x^2} \quad (9)$$

and

$$\mu' \frac{\partial U_t'}{\partial r} + \sigma \frac{\partial^2 \xi}{\partial r^2} = \mu'' \frac{\partial U_t''}{\partial r} \quad (10)$$

If the surface tension is negligible and the viscosity of vapor is very much smaller than that of liquid, Eqs. (9) and (10) reduce to

$$P'' = P' \quad (11)$$

and

$$\frac{\partial U_t'}{\partial r} = 0 \quad (12)$$

These equations are the conditions for an ideal flow.

If the viscous-heating, pressure work, convection in the radial direction, conduction along the bubble surface and $\frac{2}{r} \left(\frac{\partial \theta}{\partial r} \right)$ near the bubble surface are all negligible, the energy equation for the liquid may be expressed as

$$\frac{\partial \theta}{\partial t} + U \frac{\partial \theta}{\partial x} = \alpha \frac{\partial^2 \theta}{\partial r^2} \quad (13)$$

The assumption of small $\frac{2}{r} \left(\frac{\partial \theta}{\partial r} \right)$ near the bubble surface is justified since the term is the order of $\frac{2}{R} \left(\frac{\partial \theta}{\partial r} \right)_{r=R}$. The latter is small compared with $\frac{\partial^2 \theta}{\partial r^2}$ if the thermal boundary-layer thickness is sufficiently small compared with R , which is the case for large Peclet number. The appropriate initial and boundary conditions are

$$\left. \begin{aligned} \theta(R, x, t) &= 1 \\ \theta(\infty, x, t) &= 0 \\ \theta(r, x, 0) &= 0 \\ \theta(r, 0, t) &= 0 \end{aligned} \right\} \quad (14)$$

The energy balance at the bubble surface requires

$$-\int_0^{\pi R} \left(\frac{\partial \theta}{\partial r} \right)_{r=R} \sin \left(\frac{x}{R} \right) dx = \frac{2R\dot{R}}{R} \frac{\rho'' L}{T_\infty - T_s} \quad (15)$$

With U in Eq. (13) specified as Eq. (2) for the quasi-steady case $\dot{U}/U \ll 1$ and as Eq. (3) for the large acceleration case $\dot{U}/U \gg 1$, Eq. (13) subject to Eqs. (14) and (15) may be solved for various case as follows:

1. Temperature Distribution

a. Quasi-Steady Case, $\dot{U}/U \ll 1$. — For the quasi-steady case in which $\dot{U}, \ddot{U}, \dots, R, \dot{R}, \ddot{R}, \dots$ are very small compared with U , and $X/U \ll 1$ in the neighborhood of the bubble surface, the following dimensionless parameters are introduced:

$$\begin{aligned} \eta = (r-R) \sqrt{\frac{U}{\alpha X}} & ; \quad \tau_0 = \dot{R} \sqrt{\frac{U}{\alpha X}} \left(\frac{X}{U} \right) ; \quad \tau_1 = \ddot{R} \sqrt{\frac{U}{\alpha X}} \left(\frac{X}{U} \right)^2 ; \quad \tau_2 = \dddot{R} \sqrt{\frac{U}{\alpha X}} \left(\frac{X}{U} \right)^3 ; \dots \\ \xi_0 = \frac{\dot{U}}{U} \left(\frac{X}{U} \right) & ; \quad \xi_1 = \frac{\ddot{U}}{U} \left(\frac{X}{U} \right)^2 ; \quad \xi_2 = \frac{\ddot{\ddot{U}}}{U} \left(\frac{X}{U} \right)^3 ; \dots \end{aligned} \quad (16)$$

If the parameters $\{\tau_0, \tau_1, \dots\}$, $\{\xi_0, \xi_1, \dots\}$ are sufficiently small, the dimensionless temperature θ may be expanded into the Taylor's series as

$$\begin{aligned} \theta &= F(\eta, \tau_i, \xi_i) \\ &= F_0(\eta) + \sum_{i=0}^{\infty} \tau_i F_i'(\eta) + \sum_{i=0}^{\infty} \sum_{j=0}^{\infty} \tau_i \tau_j F_{ij}^2(\eta) + \dots \\ &+ \sum_{i=0}^{\infty} \xi_i f_i'(\eta) + \sum_{i=0}^{\infty} \sum_{j=0}^{\infty} \xi_i \xi_j f_{ij}^2(\eta) + \dots \quad (17) \\ &+ \sum_{i=0}^{\infty} \sum_{j=0}^{\infty} \tau_i \xi_j D_{ij}^2(\eta) + \dots \\ &+ \dots \end{aligned}$$

The substitution of Eq. (17) into Eqs. (13) and (14) followed by collecting the same order of the terms yields the following simultaneous ordinary differential equations with their appropriate boundary conditions.

0th Order

$$\frac{\eta}{2} \dot{F}_0^0 + \ddot{F}_0^0 = 0$$

B.C.s. $F_0^0(0) = 1, F_0^0(\infty) = 0$

1st Order

$$\tau_0: -\frac{\eta}{2} \dot{F}_0^1 - \dot{F}_0^0 + \frac{F_0^1}{2} - \ddot{F}_0^1 = 0$$

B.C.s. $F_0^1(0) = F_0^1(\infty) = 0$

$$\tau_1: -\frac{\eta}{2} \dot{F}_1^1 + F_0^1 + \frac{3}{2} F_1^1 - \ddot{F}_1^1 = 0$$

$F_1^1(0) = F_1^1(\infty) = 0$

$$\tau_2: -\frac{\eta}{2} \dot{F}_2^1 + F_1^1 + \frac{5}{2} F_2^1 - \ddot{F}_2^1 = 0$$

$F_2^1(0) = F_2^1(\infty) = 0$

...

$$\xi_0: -\frac{\eta}{2} \dot{f}_0^1 + f_0^1 + \frac{\eta}{2} \dot{F}_0^0 - \ddot{f}_0^1 = 0$$

$f_0^1(0) = f_0^1(\infty) = 0$

$$\xi_1: -\frac{\eta}{2} \dot{f}_1^1 + f_0^1 + 2f_1^1 - \ddot{f}_1^1 = 0$$

$f_1^1(0) = f_1^1(\infty) = 0$

$$\xi_2: -\frac{\eta}{2} \dot{f}_2^1 + f_1^1 + 3f_2^1 - \ddot{f}_2^1 = 0$$

$f_2^1(0) = f_2^1(\infty) = 0$

...

2nd Order

$$(\tau_0)^2: -\frac{\eta}{2} \dot{F}_{00}^2 - \dot{F}_0^1 + F_{00}^2 - \ddot{F}_{00}^2 = 0$$

B.C.s $F_{00}^2(0) = F_{00}^2(\infty) = 0$

$$\tau_0 \tau_1: -\dot{F}_1^1 - \eta \dot{F}_{01}^2 + 2F_{00}^2 + 4F_{01}^2 - 2\ddot{F}_{01}^2 = 0$$

$F_{01}^2(0) = F_{01}^2(\infty) = 0$

$$(\tau_1)^2: -\frac{\eta}{2} \dot{F}_{11}^2 + 2F_{01}^2 + 3F_{11}^2 - \ddot{F}_{11}^2 = 0$$

$F_{11}^2(0) = F_{11}^2(\infty) = 0$

...

$$(\xi_0)^2: \frac{\eta}{2} \dot{f}_0^1 - \frac{\eta}{2} \dot{f}_{00}^2 - 2f_0^1 + 2f_{00}^2 - \ddot{f}_{00}^2 = 0$$

$f_{00}^2(0) = f_{00}^2(\infty) = 0$

$$\tau_0 \xi_0: -f_0^1 + \frac{\eta}{2} \dot{F}_0^1 - \frac{\eta}{2} \dot{D}_{00}^2 - F_0^1/2 + \frac{3}{2} D_{00}^2 - \ddot{D}_{00}^2 = 0$$

$D_{00}^2(0) = D_{00}^2(\infty) = 0$

$$\xi_0 \xi_1: -\eta f_{01}^2 + \frac{\eta}{2} \dot{f}_1^1 + 6f_{11}^2 + 2f_{00}^2 - 3f_1^1 - 2\dot{f}_{01}^2 = 0$$

$f_{01}^2(0) = f_{01}^2(\infty) = 0$

$$(\xi_1)^2: -\frac{\eta}{2} \dot{f}_{11}^2 + 2f_{01}^2 + 4f_{11}^2 - \ddot{f}_{11}^2 = 0$$

$f_{11}^2(0) = f_{11}^2(\infty) = 0$

$$\tau_0 \xi_1: -f_1^1 - \frac{\eta}{2} \dot{D}_{01}^2 + D_{00}^2 + \frac{5}{2} D_{01}^2 - \ddot{D}_{01}^2 = 0$$

$D_{01}^2(0) = D_{01}^2(\infty) = 0$

$$\tau_1 \xi_0: -\frac{\eta}{2} \dot{F}_1^1 - \frac{\eta}{2} \dot{D}_{10}^2 + D_{00}^2 - \frac{3}{2} F_1^1 + \frac{5}{2} D_{10}^2 - \ddot{D}_{10}^2 = 0$$

$D_{10}^2(0) = D_{10}^2(\infty) = 0$

...

(18)

b. Large Acceleration Case, $\dot{U}/U \gg 1$.--New dimensionless parameters are defined for Eq. (17) as

$$\eta = (r-R) \sqrt{\frac{\dot{U}}{\alpha U}} \quad ; \quad \tau_0 = \dot{R} \sqrt{\frac{\dot{U}}{\alpha U}} \left(\frac{U}{\dot{U}}\right) \quad ; \quad \tau_1 = \dot{R} \sqrt{\frac{\dot{U}}{\alpha U}} \left(\frac{U}{\dot{U}}\right)^2 \quad ; \quad \tau_2 = \ddot{R} \sqrt{\frac{\dot{U}}{\alpha U}} \left(\frac{U}{\dot{U}}\right) \quad ; \quad \dots \quad (19)$$

$$\xi_0 = \left(\frac{U}{\dot{U}}\right) \left(\frac{\ddot{U}}{\dot{U}}\right) \quad ; \quad \xi_1 = \left(\frac{U}{\dot{U}}\right)^2 \frac{\ddot{U}}{\dot{U}} \quad ; \quad \xi_2 = \left(\frac{U}{\dot{U}}\right) \left(\frac{\ddot{U}}{\dot{U}}\right) \quad ; \quad \dots$$

Following the same procedure as described in the previous section a set of ordinary differential equations and their appropriate boundary conditions are obtained. They are identical with Eqs. (18) except for the boundary condition at $X = 0$, which cannot be satisfied for this case.

2. Solution for the Bubble Growth Rate

a. Quasi-Steady Case, $\dot{U}/U \ll 1$.--The energy balance at the bubble surface as given by Eq. (15) may be expressed as

$$-\int_0^\pi \left. \frac{\partial \theta}{\partial \eta} \right|_{\eta=0} \sqrt{\frac{U}{\alpha X}} \sin\left(\frac{X}{R}\right) d\left(\frac{X}{R}\right) = \frac{2 \rho'' L}{h(T_\infty - T_s)} \dot{R}$$

With the substitution of Eq. (17), the above equation becomes

$$-\int_0^\pi \sqrt{\frac{U}{\alpha X}} \sin\left(\frac{X}{R}\right) \left[\dot{F}_0^0(0) + \tau_1 \dot{F}_1^1(0) + \tau_1 \tau_2 \dot{F}_{12}^2(0) + \dots \right. \\ \left. + \xi_1 \dot{f}_1^1(0) + \xi_1 \xi_2 \dot{f}_{12}^2(0) + \dots + \tau_1 \xi_2 \dot{D}_{12}^2(0) + \dots \right] d\left(\frac{X}{R}\right) \quad (20)$$

$$= 2 \frac{L \rho''}{h(T_\infty - T_s)} \dot{R}$$

where the parameters, as defined in Eq. (16), may be rewritten as

$$\begin{aligned}
\tau_0 &= \dot{r} \sqrt{Pe} \left(\frac{Br}{u} \right)^{1/2} \\
\tau_1 &= \ddot{r} \sqrt{Pe} \left(\frac{Br}{u} \right)^{3/2} \\
\tau_2 &= \dddot{r} \sqrt{Pe} \left(\frac{Br}{u} \right)^{5/2} \\
&\dots \\
\xi_0 &= \left(\frac{Br}{u} \right) \frac{\dot{u}}{u} \\
\xi_1 &= \left(\frac{Br}{u} \right)^2 \frac{\ddot{u}}{u} \\
\xi_2 &= \left(\frac{Br}{u} \right)^3 \frac{\dddot{u}}{u} \\
&\dots
\end{aligned} \tag{21}$$

The relationship between the bubble growth rate and translatory velocity may be obtained from Eq. (2) as

$$\begin{aligned}
\frac{\dot{u}}{u} &= 2 \frac{\dot{r}}{r} \\
\frac{\ddot{u}}{u} &= 2 \frac{(r\ddot{r} + \dot{r}^2)}{r^2} \\
\frac{\dddot{u}}{u} &= \frac{2(r\dddot{r} + 3\dot{r}\ddot{r})}{r^2} \\
\frac{u}{r} &= r
\end{aligned} \tag{22}$$

Substituting the combination of Eqs. (20)-(22) gives

$$\begin{aligned}
& \int_0^\pi \sqrt{Pe} \sin \beta \left[\dot{F}_0'(0) + \dot{F}_0'(0) \dot{r} \sqrt{Pe} \left(\frac{\beta}{r}\right)^{1/2} + F_1'(0) \ddot{r} \sqrt{Pe} \left(\frac{\beta}{r}\right)^{3/2} + F_2'(0) \ddot{r} \sqrt{Pe} \left(\frac{\beta}{r}\right)^{5/2} + \dots \right. \\
& \quad + 2 \dot{f}_0'(0) \left(\frac{\beta}{r}\right) \frac{\dot{r}}{r} + 2 \dot{f}_1'(0) \left(\frac{\beta}{r}\right)^2 \frac{r \ddot{r} + \dot{r}^2}{r^2} + 2 \dot{f}_2'(0) \left(\frac{\beta}{r}\right)^3 \frac{(r \ddot{r} + 3 \dot{r} \dot{r}')}{r^2} + \dots \\
& \quad + \dot{F}_{00}''(0) Pe \left(\frac{\beta}{r}\right) \dot{r}^2 + 2 \dot{F}_{01}''(0) Pe \left(\frac{\beta}{r}\right)^2 \dot{r} \ddot{r} + \dot{F}_{11}''(0) Pe \left(\frac{\beta}{r}\right)^3 \dot{r}'^2 + \dots \\
& \quad + 4 \dot{f}_{00}''(0) \left(\frac{\beta}{r}\right)^2 \frac{\dot{r}'^2}{r^2} + 8 \dot{f}_{01}''(0) \left(\frac{\beta}{r}\right)^3 \frac{\dot{r} (r \ddot{r} + \dot{r}^2)}{r^3} + 4 \dot{f}_{11}''(0) \left(\frac{\beta}{r}\right)^4 \frac{(r \ddot{r} + \dot{r}^2)^2}{r^4} + \dots \\
& \quad + 2 D_{00}^3(0) \sqrt{Pe} \left(\frac{\beta}{r}\right) \frac{\dot{r}^2}{r} + 2 D_{01}^3(0) \sqrt{Pe} \left(\frac{\beta}{r}\right)^2 \frac{(r \ddot{r} + \dot{r}^2) \dot{r}}{r^2} + 2 D_{10}^3(0) \sqrt{Pe} \frac{\dot{r} \dot{r}'}{r} + \dots \\
& \quad \left. \dots \right] d\beta = -2 Pe \delta \dot{r}
\end{aligned}$$

(23)

Integrating Eq. (23) followed by the substitution of $\dot{F}_0'(0)$, $\dot{F}_0'(0)$, \dots numerically obtained by solving Eqs. (18) one obtains the ordinary differential equation in r as

$$\begin{aligned}
& -1.010616 r^6 - 1.0040 \sqrt{Pe} \dot{r} r^{1/2} + 0.390204 \sqrt{Pe} \ddot{r} r^{9/2} - 0.18146 \sqrt{Pe} \ddot{r}' r^{7/2} + \dots \\
& \quad + 0.69097 \dot{r} r^4 - 0.39473 (r^3 \ddot{r} + \dot{r} r^2) + 0.193804 (r^2 \ddot{r}' + 3 r \dot{r} \dot{r}') + \dots \\
& \quad - 0.3537 Pe \dot{r}^2 r^5 + 0.20603 Pe \dot{r} \ddot{r} r^4 + 0.016466 Pe \ddot{r}'^2 r^3 + \dots \\
& \quad + 1.47536 \dot{r}'^2 r^2 - 2.70748 (r \dot{r} \ddot{r} + \dot{r}^3) + 1.240259 \frac{(r^2 \dot{r}'^2 + \dot{r}^4 + 2 r \dot{r} \dot{r}')}{r^2} \\
& \quad + 0.0128988 \sqrt{Pe} \dot{r}^2 r^{7/2} - 0.019216 \sqrt{Pe} (r \dot{r} \ddot{r} + \dot{r}^3) r^{3/2} + 0.701526 \sqrt{Pe} \dot{r} \ddot{r}' r^{5/2} \\
& \quad + \dots + 2 \delta \sqrt{Pe} \dot{r} r^{1/2} = 0
\end{aligned}$$

(24)

Equation (24) expresses the response of the bubble growth or collapse caused by a step change in the translatory velocity and/or the boundary movement of the bubble. Since the dimensionless temperature θ is expanded into a power series as Eq. (17), Eq. (24) consists of an infinite number of terms. The number of terms necessary to be taken in Eq. (24) depends on the convergence of the θ power-series.

In general, the power-series method assumes that the solution exists and is analytic in a certain region in which a power-series to represent it is formally setup at the beginning of the procedure. The uniqueness and the exact region of convergence would have to be given by subsequent proofs. This may be reasonably assessed by studying the behavior of the series when the number of terms included is varied. The technique is to be applied to Eq. (24). Equation (24) has been numerically solved for the following cases by means of an IBM 7090 digital computer:

Case 1. Zeroth-order solution, which retains no terms involving τ_i and ξ_i . Equation (24) reduces to

$$\frac{dr}{d\tau} = \frac{0.50503}{\delta \times \sqrt{Pe}} r^{1/2} \quad (25)$$

subject to the initial condition $r_0 = 1.0$. Equation (25) is integrated to give

$$r = \left(1 + \frac{0.50503}{\delta \times \sqrt{Pe}} \tau \right)^2 \quad (26)$$

Case 2. First-order, first-power solution, which retains those terms involving the zeroth-order solution and τ_0, ξ_0 . Equation (24) becomes

$$\frac{dr}{d\tau} = \frac{1.010615 r^2}{(2\delta - 1.004052)\sqrt{Pe} r^{3/2} + 0.690978} \quad (27)$$

Case 3. First-order, second-power solution, which retains those terms involving the zeroth-order solution and $\tau_0, \xi_0, \tau_0^2, \xi_0^2, \tau_0 \xi_0$. Equation (24) reduces to

$$\frac{dr}{d\tau} = -\frac{B1}{2A1} + \frac{I}{2A1} \sqrt{B1^2 - 4A1 \times C1} \quad (28)$$

where

$$A1 = -0.35370 Pe r^5 + 1.47536 r^2 + 0.012899 \sqrt{Pe} r^{7/2}$$

$$B1 = (28 - 1.004052) \sqrt{Pe} r^{11/2} + 0.690978 r^4$$

$$C1 = -1.0106156 r^6$$

Case 4. Second-order, first-power solution, which retains those terms involving the zeroth-order solution and $\zeta_0, \zeta_1, \xi_0, \xi_1$. Equation (24) becomes

$$\ddot{r} = -C2/B2 \quad (29)$$

where

$$A2 = 0.0164664 Pe r^3 + 1.24026$$

$$B2 = 0.390204 \sqrt{Pe} r^{9/2} - 0.39473 r^3 - (2.12607 r - 0.20603 Pe r^4 - 0.68231 \sqrt{Pe} r^{5/2}) \dot{r} + 2.4805 \dot{r}^2 / r$$

$$C2 = -1.010616 r^6 + \dot{r} [(28 - 1.00405) \sqrt{Pe} r^{11/2} + 0.690978 r^4] + \dot{r}^2 (-0.35370 Pe r^5 + 1.08063 r^2 + 0.012899 \sqrt{Pe} r^{7/2}) - \dot{r}^3 (2.70748 + 0.01921 \sqrt{Pe} r^{3/2}) + 1.240259 \dot{r}^4 / r^2$$

$$D2 = -0.18146 \sqrt{Pe} r^{7/2} + 0.193804 r^2$$

Case 5. Second-order, second-power solution, which retains those terms involving the zeroth-order solution and $\tau_0, \tau_1, \tau_0^2, \tau_0\tau_1, \tau_0\xi_0, \tau_0\xi_1, \tau_1\xi_0, \xi_0, \xi_1, \xi_0^2, \xi_1^2, \xi_0\xi_1$

One obtains

$$\ddot{r} = -\frac{B_2}{2 \cdot A_2} - \frac{1}{2 \cdot A_2} \sqrt{B_2^2 - 4 \cdot A_2 \cdot C_2} \quad (30)$$

Case 6. Third-order, first-power solution, which retains those terms involving Case 5 and ξ_2 .

One obtains

$$\ddot{r} = -\frac{A_2 \cdot \ddot{r}^2 + B_2 \cdot \ddot{r} + C_2}{D_2} \quad (31)$$

b. Large Acceleration Case, $\dot{U}/U \gg 1$.—The bubble motion was investigated for the early period when the bubble starts upward translatory motion from rest by Miyagi⁵ as

$$U_\infty = U_0 \left(1 - \frac{2}{1 + e^{kt}} \right) \quad (32)$$

Miyagi⁵ verified Eq. (1) both experimentally and theoretically employing the concept of "added mass."

From Eq. (3), the following relationships are obtained.

$$\frac{U}{\dot{U}} = \frac{(1 + e^{kt})(e^{kt} - 1)}{2 e^{kt}}$$

$$\frac{\ddot{U}}{\dot{U}} = \frac{(1 - e^{kt})}{1 + e^{kt}}$$

$$\frac{\ddot{\ddot{U}}}{\dot{U}} = \frac{1 - 4e^{kt} + e^{2kt}}{(1 + e^{kt})^2}$$

...

In the region $\kappa t \ll 1$, one obtains

$$\frac{U}{\dot{U}} \approx t + \frac{3}{2} \kappa t^2 + \dots$$

$$\frac{\ddot{U}}{U} \approx -\kappa (2\kappa t - \kappa^2 t^2 + \dots)$$

...

$$\xi_0 = \frac{U}{\dot{U}} \frac{\ddot{U}}{U} = -\frac{(1 - e^{-\kappa t})^2}{2e^{\kappa t}} \approx -\frac{\kappa^2 t^2}{2} = -\frac{\gamma^2 \tau^2}{2}$$

$$\xi_1 = \left(\frac{U}{\dot{U}}\right)^2 \frac{\ddot{U}}{U} = -\frac{(e^{\kappa t} - 1)^2 (-1 + 4e^{\kappa t} - e^{2\kappa t})}{4e^{2\kappa t}} \approx -\frac{\kappa^2 t^2}{2} = -\frac{\gamma^2 \tau^2}{2}$$

$$\xi_2 = \left(\frac{U}{\dot{U}}\right)^3 \frac{\ddot{U}}{U} = \frac{(e^{\kappa t} - 1)^3 (-1 + 11e^{2\kappa t} - e^{3\kappa t})}{8e^{3\kappa t}} \approx -\kappa^4 t^4 = -\gamma^4 \tau^4$$

...

$$\tau_0 = R \sqrt{\frac{\dot{U}}{\alpha U}} \left(\frac{U}{\dot{U}}\right) = r \sqrt{Pe} \tau^{1/2}$$

$$\tau_1 = \ddot{r} \sqrt{Pe} \tau^{3/2}$$

$$\tau_2 = \ddot{\ddot{r}} \sqrt{Pe} \tau^{5/2}$$

...

The time required to reach 95% of the steady-state velocity may be calculated from Eq. (3) as

$$\tau_{\text{steady}} = \frac{1}{\gamma} \ln \frac{U_0 + U_{95\%}}{U_0 - U_{95\%}} = \frac{1}{\gamma} \ln 39$$

The same procedure is followed to calculate the bubble dynamics as given in V-B-2-a. One obtains

$$\begin{aligned}
& 0.564589 + (0.50487 - \delta) \sqrt{Pe} \tau^{1/2} \dot{\gamma} - 0.1232306 \sqrt{Pe} \tau^{3/2} \ddot{\gamma} + \dots \\
& + 0.007162 \delta^2 \tau^2 - 0.02320 \delta^2 \tau^2 + 0.01141 \delta^2 \tau^4 + \dots \\
& - 0.15653 \dot{\gamma}^2 Pe \tau - 0.02570 \dot{\gamma} \ddot{\gamma} Pe \tau^4 + 0.00142 \ddot{\gamma}^2 Pe \tau^6 + \dots \\
& - 0.005327 \dot{\gamma} \ddot{\gamma} \sqrt{Pe} \tau^{5/2} + 0.0008 \ddot{\gamma} \dot{\gamma} \sqrt{Pe} \tau^{5/2} - 0.03 \ddot{\gamma} \dot{\gamma} Pe \tau^{5/2} + \dots \\
& = 0
\end{aligned}$$

(33)

Case 1. First-order solution. Assuming $\dot{\gamma} \gg \ddot{\gamma}$, $\dot{\gamma} \ll 1$, and $\delta \gg 1$ and $\tau \ll 1$, Eq. (33) becomes

$$\dot{\gamma} = \frac{1}{(\delta - 0.50487) \sqrt{Pe} \sqrt{\tau}} (0.564589 + 0.0484 \tau^2 \delta^2)$$

The integration gives

$$\gamma = 1 + \frac{1}{\sqrt{Pe} (\delta - 0.50487)} (1.129178 \sqrt{\tau} + 0.0678 \delta^2 \tau^{5/2}) \quad (34)$$

Case 2. Second-order solution. Including the τ^2 term Eq. (33) may be re-written as

$$\ddot{\gamma} = \frac{0.564589 + \dot{\gamma}(0.50487 - \delta) \sqrt{Pe} \sqrt{\tau} + 0.1516 Pe \tau \dot{\gamma}^2 + 0.0484 \delta^2 \tau^2}{0.025701 Pe \tau^2 \dot{\gamma} + 0.12323 \sqrt{Pe} \tau^{3/2} + 0.03 \sqrt{Pe} \dot{\gamma} \tau^{5/2}} \quad (35)$$

C. RESULTS AND DISCUSSION

1. Temperature Distribution

A set of simultaneous ordinary differential equations, Eqs. (18) with their appropriate boundary conditions are solved numerically by steps of 0.01 using an IBM 7090 digital computer. The method of Runge and Kutta was employed for this purpose. The temperature distribution functions F and f are graphically presented in Figs. 19-21. These functions may be physically interpreted as follows:

$F_0^0(\eta)$: Temperature distribution function for steady state which corresponds to a constant size bubble in translatory motion with a constant velocity.

$F_0^1(\eta)$: Temperature component influenced by the bubble growth speed as expressed by the parameter τ_0 .

$F_1^1(\eta)$: Temperature component influenced by the bubble growth acceleration as expressed by the parameter τ_1 .

...

f_0^1 : Temperature component influenced by the bubble translatory speed acceleration as expressed by the parameter ξ_0 .

...

In order to evaluate the effects of the boundary-layer motion and/or translatory variation on the temperature distribution, it is essential to know the magnitude of each parameter. Among these parameters, τ_0 , τ_1 , and ξ_0 have larger effects on the temperature distribution than the others. It is disclosed that the parameters τ_0 , τ_2 have a positive effect on the bubble growth while τ_1 has a negative effect. Those parameters which indicate the effect of the translatory-velocity variation, ξ_0 , ξ_1 , tend to suppress the bubble growth. If both R and U are positive, their effects on the bubble growth are opposite and may cancel each other, although the effect of R appears greater.

2. Bubble Growth or Collapse

For the quasi-steady case, the time-history of bubble growth is presented in Fig. 22 as a function of the dimensionless parameter δ . It is seen that the convergence of the solution is quite rapid for $\delta > 2$. However, when δ becomes less than unity the solution has poor convergence because the assumption of small τ_0 , τ_1 , fails when δ is too small since the temperature and \dot{r} difference becomes large.

For the large acceleration case the bubble growth rate is presented in Figs. 22 and 23 for a comparison with the quasi-steady case. A faster growth rate is recorded. Figure 24 shows the convergence of the bubble dynamic Eq. (33). A poor convergence is observed as δ becomes less than unity.

D. CONCLUSIONS

1. The technique developed evaluates the effects of the boundary movement and translatory velocity change of the spherical bubble on the temperature field and the bubble growth rate.

2. A substantially higher growth rate is obtained for the case of large acceleration compared with the quasi-steady case.

3. The bubble growth for small δ varies with t^2 compared with $t^{1/2}$ for the growth of a stationary bubble in a superheated liquid.

4. The present solutions converge very well for $\delta > 1$ for both small and large acceleration.

Page intentionally left blank

VI. TRANSIENT, LAMINAR FREE CONVECTION HEAT TRANSFER IN TWO-DIMENSIONAL CONTAINERS

A. ANALYTICAL WORK

The numerical method of finite-difference approximation, described in Ref. 7, for the solution of transient, laminar free convection heat and mass transfer in two-dimensional rectangular liquid containers, is used for the solution of the transient natural convection velocity and temperature distributions in cylindrical containers. In applying the previously described method to the new geometry, some modifications of the computational procedures, as well as in the difference-equations, were required owing to the difference in the geometry. The development of the differential equations, difference-equations and the boundary conditions is given below. The fluid is assumed to be incompressible and the properties are constant. Density variations are allowed, in the axial-momentum equation, only in the body force term where density differences give rise to the buoyancy force. The geometry is given in Fig. 25.

The Differential Equations:

X-momentum

$$\rho \left(\frac{\partial u}{\partial t} + u \frac{\partial u}{\partial x} + v \frac{\partial u}{\partial r} \right) = -\rho g - \frac{\partial p}{\partial x} + \mu \left[\frac{\partial^2 u}{\partial x^2} + \frac{1}{r} \frac{\partial u}{\partial r} + \frac{\partial^2 u}{\partial r^2} \right] \quad (36)$$

Radial momentum equation

$$\rho \left(\frac{\partial v}{\partial t} + u \frac{\partial v}{\partial x} + v \frac{\partial v}{\partial r} \right) = -\frac{\partial p}{\partial r} + \mu \left[\frac{\partial^2 v}{\partial x^2} + \frac{1}{r} \frac{\partial v}{\partial r} + \frac{\partial^2 v}{\partial r^2} \right] \quad (37)$$

Continuity equation

$$\frac{\partial u}{\partial x} + \frac{v}{r} + \frac{\partial v}{\partial r} = 0 \quad (38)$$

Energy equation

$$\frac{\partial T}{\partial t} + u \frac{\partial T}{\partial x} + v \frac{\partial T}{\partial r} = \alpha \left[\frac{\partial^2 T}{\partial x^2} + \frac{1}{r} \frac{\partial T}{\partial r} + \frac{\partial^2 T}{\partial r^2} \right] \quad (39)$$

Differentiating the x-momentum with respect to r and the r-momentum with respect to x, eliminating the pressure term the following equation is obtained:

$$\begin{aligned} & \frac{\partial}{\partial t} \left(\frac{\partial u}{\partial r} - \frac{\partial z}{\partial x} \right) + u \frac{\partial}{\partial x} \left(\frac{\partial u}{\partial r} - \frac{\partial z}{\partial x} \right) + z \frac{\partial}{\partial r} \left(\frac{\partial u}{\partial r} - \frac{\partial z}{\partial x} \right) + \\ & \left(\frac{\partial u}{\partial r} - \frac{\partial z}{\partial x} \right) \left(\frac{\partial u}{\partial x} + \frac{\partial z}{\partial r} \right) = -\frac{1}{\rho} g \frac{\partial \rho}{\partial r} + \nu \left[\frac{\partial^2}{\partial x^2} \left(\frac{\partial u}{\partial r} - \frac{\partial z}{\partial x} \right) + \right. \\ & \left. \frac{\partial^2}{\partial r^2} \left(\frac{\partial u}{\partial r} - \frac{\partial z}{\partial x} \right) + \frac{1}{r} \left(\frac{\partial u}{\partial r} - \frac{\partial z}{\partial x} \right) \right] \end{aligned} \quad (40)$$

since the pressure changes are small, then the density variations could be assumed a function of temperature only. The following relationship is always used:

$$P = P_0 [1 + \beta(T_0 - T)] \quad (41)$$

where ρ_0 and T_0 are the initial values of the density and temperature, respectively.

From the continuity equation

$$\frac{\partial u}{\partial x} + \frac{\partial z}{\partial r} = -\frac{z}{r} \quad (42)$$

also let

$$W' = \frac{\partial u}{\partial r} - \frac{\partial z}{\partial x} \quad (43)$$

substituting Eqs. (41)-(43) in (40) we get:

$$\frac{\partial W'}{\partial t} + u \frac{\partial W'}{\partial x} + z \frac{\partial W'}{\partial r} - \frac{z W'}{r} = g \beta \frac{\partial T}{\partial r} + \nu \left[\frac{\partial^2 W'}{\partial x^2} + \frac{1}{r} \frac{\partial W'}{\partial r} + \frac{\partial^2 W'}{\partial r^2} \right] \quad (44)$$

since the velocity component changes sign in the two-dimensional domain considered, the presence of the term $(z W'/r)$ in Eq. (9) presents a computa-

tional stability problem. A possible solution for this problem could be made by taking the value of $(\partial w / \partial r)$ to be that at the advanced time level if v is positive, and is evaluated at the present time level if v is negative. One disadvantage of this procedure is that this term is not evaluated at the same time level at all nodal points. However, a different approach was made to handle this problem, by which this term is eliminated from Eq. (45) in the following way:

Let:

$$w'' = \frac{w'}{r} \quad (45)$$

Upon substitution of Eq. (45) in (44), Eq. (44) is reduced to the following form:

$$\frac{\partial w''}{\partial t} + u \frac{\partial w''}{\partial x} + v \frac{\partial w''}{\partial r} = g\beta \frac{1}{r} \frac{\partial T}{\partial r} + \nu \left[\frac{\partial^2 w''}{\partial z^2} + \frac{1}{r} \frac{\partial w''}{\partial r} + \frac{\partial^2 w''}{\partial r^2} \right] \quad (46)$$

where

$$w'' = \frac{1}{r} \left[\frac{\partial u}{\partial r} - \frac{\partial v}{\partial x} \right] \quad (47)$$

The substitutions necessary to nondimensionalize the equations are:

$$\begin{aligned} t &= \frac{a^2}{\alpha} t & ; & & x &= bX & ; & & r &= aR \\ u &= \frac{\alpha b}{a^4} U & ; & & v &= \frac{\alpha}{a} V & ; & & T - T_0 &= \frac{\nu \alpha b}{\beta g a^4} \Theta \end{aligned} \quad (48)$$

$$w'' = \frac{\alpha b}{a^2} W$$

Defining the stream function Ψ by:

$$\begin{aligned} U &= \frac{1}{R} \frac{\partial \Psi}{\partial R} \\ V &= - \frac{1}{R} \frac{\partial \Psi}{\partial X} \end{aligned} \quad (49)$$

Substituting (48) and (49) in (39), (46), and (47), we obtain:

$$\frac{\partial \theta}{\partial t} + U \frac{\partial \theta}{\partial X} + V \frac{\partial \theta}{\partial R} = \frac{\alpha^2}{b^2} \frac{\partial^2 \theta}{\partial R^2} + \frac{1}{R} \frac{\partial \theta}{\partial R} + \frac{\partial^2 \theta}{\partial R^2} \quad (50)$$

$$\frac{\partial W}{\partial t} + U \frac{\partial W}{\partial X} + V \frac{\partial W}{\partial R} = Pr \left[\frac{1}{R} \frac{\partial \theta}{\partial R} + \frac{\alpha^2}{b^2} \frac{\partial^2 W}{\partial X^2} + \frac{3}{R} \frac{\partial W}{\partial R} + \frac{\partial^2 W}{\partial R^2} \right] \quad (51)$$

$$W = \frac{1}{R^2} \left[\frac{\alpha^2}{b^2} \frac{\partial^2 \psi}{\partial X^2} + \frac{\partial^2 \psi}{\partial R^2} - \frac{1}{R} \frac{\partial \psi}{\partial R} \right] \quad (52)$$

The derivatives in Eqs. (50)-(52) are approximated by finite differences as follows:

1. The first order derivatives $U \frac{\partial \theta}{\partial X}$, $V \frac{\partial \theta}{\partial R}$, $U \frac{\partial W}{\partial R}$ and $V \frac{\partial W}{\partial R}$ are approximated by backward-differences if the coefficient velocity component is positive, and is represented by forward-differences if the coefficient velocity component is negative. This is the same procedure used in Ref. 7.
2. The second order derivatives $\frac{\partial^2 T}{\partial X^2}$, $\frac{\partial^2 T}{\partial R^2}$, $\frac{\partial^2 W}{\partial X^2}$ and $\frac{\partial^2 W}{\partial R^2}$ are approximated according to the following formula:

$$\frac{\partial^2 f}{\partial X^2} = \frac{f(x+\Delta x) - 2f(x) + f(x-\Delta x)}{(\Delta x)^2} \quad (53)$$

3. The first order derivatives in terms $\frac{1}{R} \frac{\partial \theta}{\partial R}$ and $\frac{3}{R} \frac{\partial W}{\partial R}$ are approximated by central derivatives.
4. Since both R and $\frac{\partial \theta}{\partial R}$ go to zero as R approached zero, then the term $\frac{1}{R} \frac{\partial \theta}{\partial R}$ in the energy equation, is replaced at the center line by its limit as the radius goes to zero.

$$\lim_{R \rightarrow 0} \frac{1}{R} \frac{\partial \theta}{\partial R} = \frac{\partial^2 \theta}{\partial R^2}$$

5. The time-derivative is represented by forward-difference, i.e.,

$$\frac{\partial f}{\partial t} \approx \frac{f(t+\Delta t) - f(t)}{\Delta t}$$

Accordingly, each of Eqs. (50), (51) and (52) can be replaced by a system of linear algebraic equations. The linearization of the algebraic equations is accomplished by assuming that U and V are known, the values of which are those at the previous time step. The difference equations for the case when $U \geq 0$, $V \geq 0$ are given below

$$\frac{\theta'_{i,j} - \theta_{i,j}}{\Delta t} + U_{i,j} \frac{\theta_{i,j} - \theta_{i-1,j}}{(\Delta X)} + V_{i,j} \frac{\theta_{i,j+1} - \theta_{i,j}}{\Delta R} = \frac{\alpha^2}{b^2} \frac{\theta_{i+1,j} - 2\theta_{i,j} + \theta_{i-1,j}}{(\Delta X)^2} + \frac{1}{R} \frac{\theta_{i,j+1} - \theta_{i,j-1}}{z(\Delta R)} + \frac{\theta_{i,j+1} - 2\theta_{i,j} + \theta_{i,j-1}}{(\Delta R)^2} \quad (54)$$

$$\frac{w'_{i,j} - w_{i,j}}{\Delta t} + U_{i,j} \frac{w_{i,j} - w_{i-1,j}}{\Delta X} + V_{i,j} \frac{w_{i,j+1} - w_{i,j}}{\Delta R} = Pr \left[\frac{1}{R} \frac{\theta'_{i,j+1} - \theta_{i,j-1}}{z\Delta R} + \frac{\alpha^2}{b^2} \frac{w_{i+1,j} - 2w_{i,j} + w_{i-1,j}}{(\Delta X)^2} + \frac{w_{i,j+1} - 2w_{i,j} + w_{i,j-1}}{(\Delta R)^2} + \frac{3}{R} \frac{w_{i,j+1} - w_{i,j-1}}{z(\Delta R)} \right] \quad (55)$$

$$w = \frac{1}{Rz} \left[\frac{\alpha^2}{b^2} \frac{\psi_{i+1,j} - 2\psi_{i,j} + \psi_{i-1,j}}{(\Delta X)^2} - \frac{1}{R} \frac{\psi_{i,j+1} - \psi_{i,j-1}}{z(\Delta R)} + \frac{\psi_{i,j+1} - 2\psi_{i,j} + \psi_{i,j-1}}{(\Delta R)^2} \right] \quad (56)$$

The primes refer to the values of the variables at the advanced time level.

The sequence of operations necessary to compute the new values of the dependent variables across any time step is summarized below.

1. Compute the new temperatures using Eq. (54).
2. The results obtained for the temperature distribution are used in Eq. (55) to calculate the new values of the vorticity W at each nodal point.
3. Equation (56) is used to find the stream functions at the interior points and could be solved by any of the known iterative methods. The block-iterative method, described in Ref. 8, is used here, since it is more efficient than the other methods.
4. The velocity components are calculated from the known stream function distribution.

5. The vorticity at the solid boundaries are calculated using the finite-difference version of Eq. (52).

It is worth mentioning that the stability criteria used for the cylindrical and the rectangular geometry are identical.

While the specific calculations described here are for step-changes, the program of computation is general and may be applied to an arbitrary time-dependent disturbance in wall heat flux. Wall temperature, ullage pressure and g-level or any simultaneous combination of these.

The method of calculations outlined above has been applied to calculate the velocity and temperature distribution in a cylindrical tank partially filled with liquid nitrogen initially at rest and at temperature T_0 and pressure P_0 . The tank walls are suddenly exposed to a constant heat flux q'' Btu/hr-ft², while the pressure in the ullage space undergoes a step change to P_s . It is assumed that the liquid surface assumes a temperature T_s which is the saturation temperature at P_s . The bottom of the tank is insulated. The ullage pressure P_s is assumed to be 50 psia. The wall heat flux q'' is equal to 400 Btu/sq ft hr.

The stream-line patterns obtained for two different values of time level are shown in Figs. 26 and 27.

B. EXPERIMENTAL WORK

Experimental work to study the phenomena of transient, laminar natural convection heat transfer in partially filled two-dimensional liquid containers is underway. The purpose of this work is to check the results obtained theoretically using the previously described technique of numerical solution. This phase of research will be completed by the end of this year.

C. ANALYTICAL STUDY OF THE VELOCITY TRANSIENTS DURING THE PRESSURIZED DISCHARGE

The numerical method used to study the transient natural convection, which has been described elsewhere (Ref. 7), is used to study the transient velocity, as well as the temperature distribution inside a two-dimensional cylindrical tank during the pressurized discharge process. Initially the fluid is at rest and the height of the liquid column is b . From this initial condition, fluid is discharged at a constant flow rate w . The discharge is assumed to continue for a period of time $t = t_d$, after which the discharge process is terminated suddenly. The time-dependent velocity as well as the transient temperature distribution during the discharge process are calculated. Also the post-shutoff velocity transients for times $t > t_d$

will be calculated and the nature of the decay of the flow currents inside the tank after the shutoff will be determined.

REFERENCES

1. Clark, J. A., H. Merte, V. S. Arpaci, et al., Pressurization of Liquid Oxygen Containers, Progress Report No. 6, ORA Report 04268-8-P, NASA Contract No. NAS-8-825, The University of Michigan, April, 1964.
2. Clark, J. A., H. Merte, V. S. Arpaci, et al., Pressurization of Liquid Oxygen Containers, Progress Report No. 2, ORA Report 04268-2-P, NASA Contract No. NAS-8-825, The University of Michigan, November, 1961.
3. Chao, B. T., "Motion of Spherical Gas Bubbles in a Viscous Liquid at Large Reynolds Number," Physics of Fluids, 3 (1962), pp. 69-79.
4. Levich, V. G., Physicochemical Hydrodynamics, Prentice-Hall, 1962.
5. Miyagi, O., "On the Motion of an Air Bubble in Water," Phil. Mag. S. 6, 50 (1925), pp. 112-140.
6. Moore, R. K., "Unsteady Laminar Boundary Layer Flows," NACA Tech. Note 2471, September, 1951.
7. Clark, J. A., and H. Z. Barakat, "Transient, Laminar, Free Convection Heat and Mass Transfer in Closed Partially Filled Liquid Containers," Tech. Report No. 1, ORA Report 04268-6-T, NASA Contract No. NAS-8-825, The University of Michigan, January, 1964.
8. Todd, J., Survey of Numerical Analysis, McGraw-Hill Book Company, 1962.
9. Larsen, P. S., and J. A. Clark, "The Dynamics of Gas-Vapor Bubbles in Binary Systems," ORA Report 04268-7-T, NASA Contract No. NAS 8-825, The University of Michigan, November, 1963.

PRECEDING PAGE BLANK NOT FILMED.

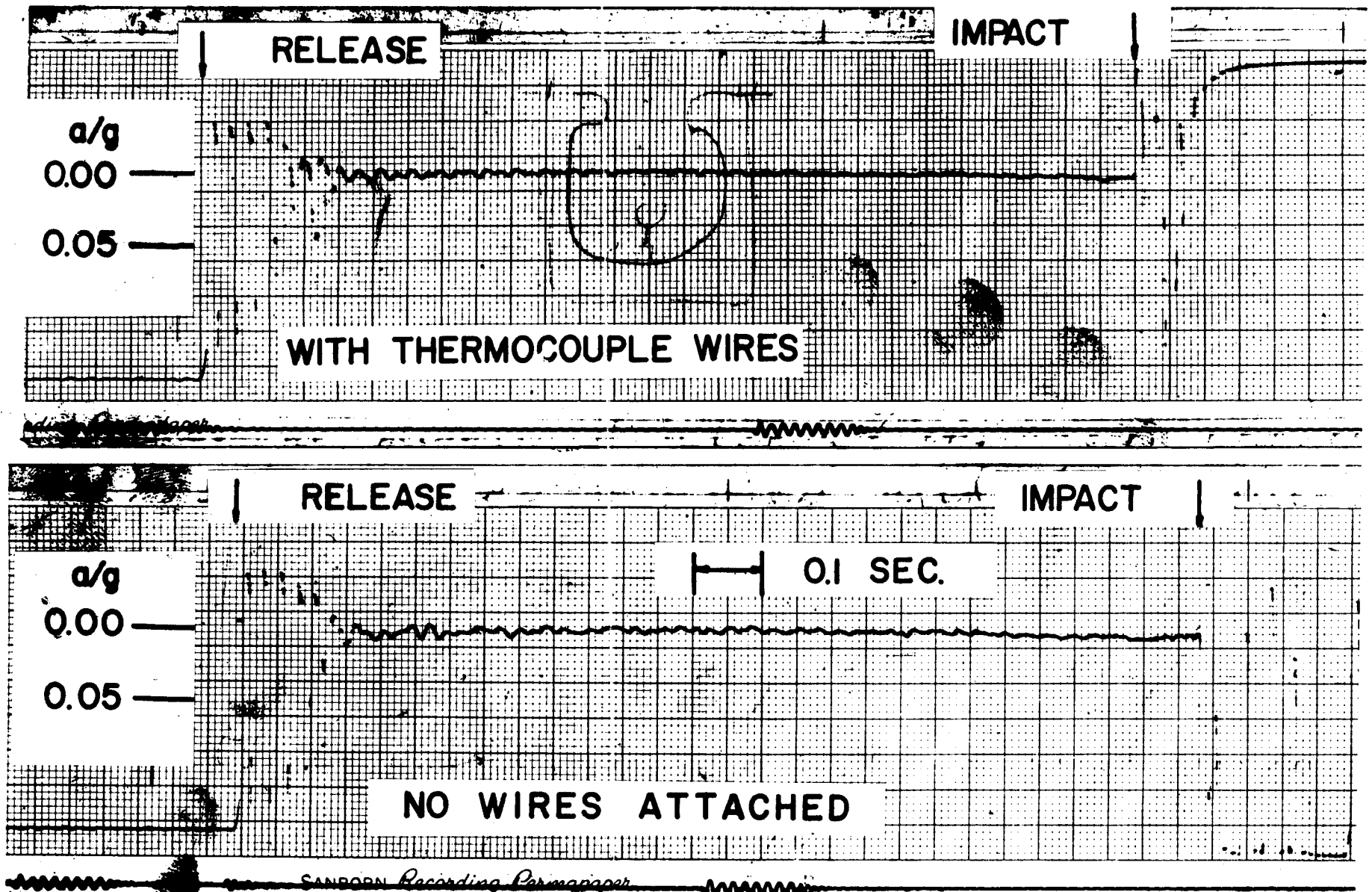


Figure 1. Accelerometer measurements on inner package.

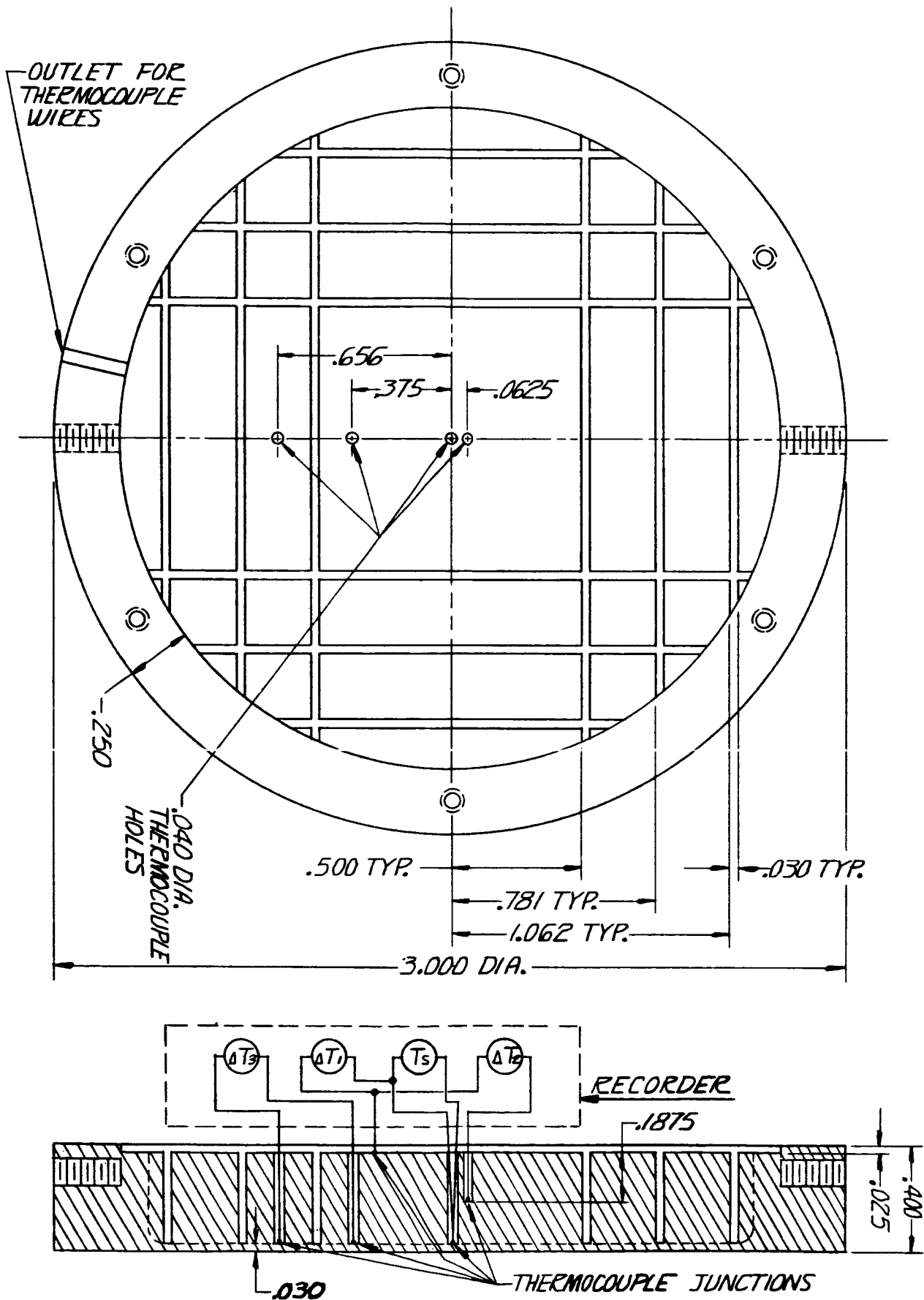


Figure 3. Modified disc for transient heat transfer measurement.

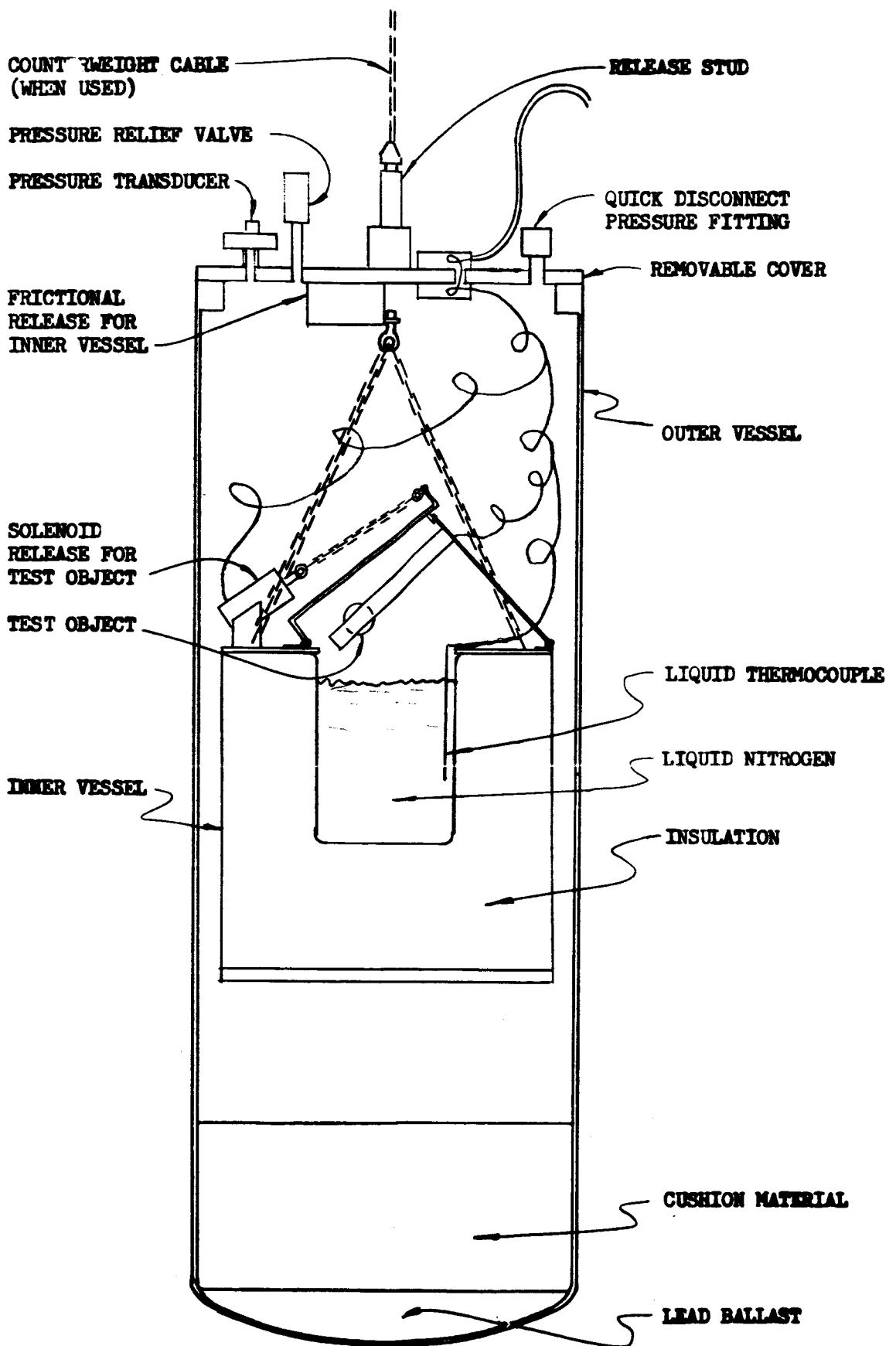


Figure 4. Pressurized test vessel.

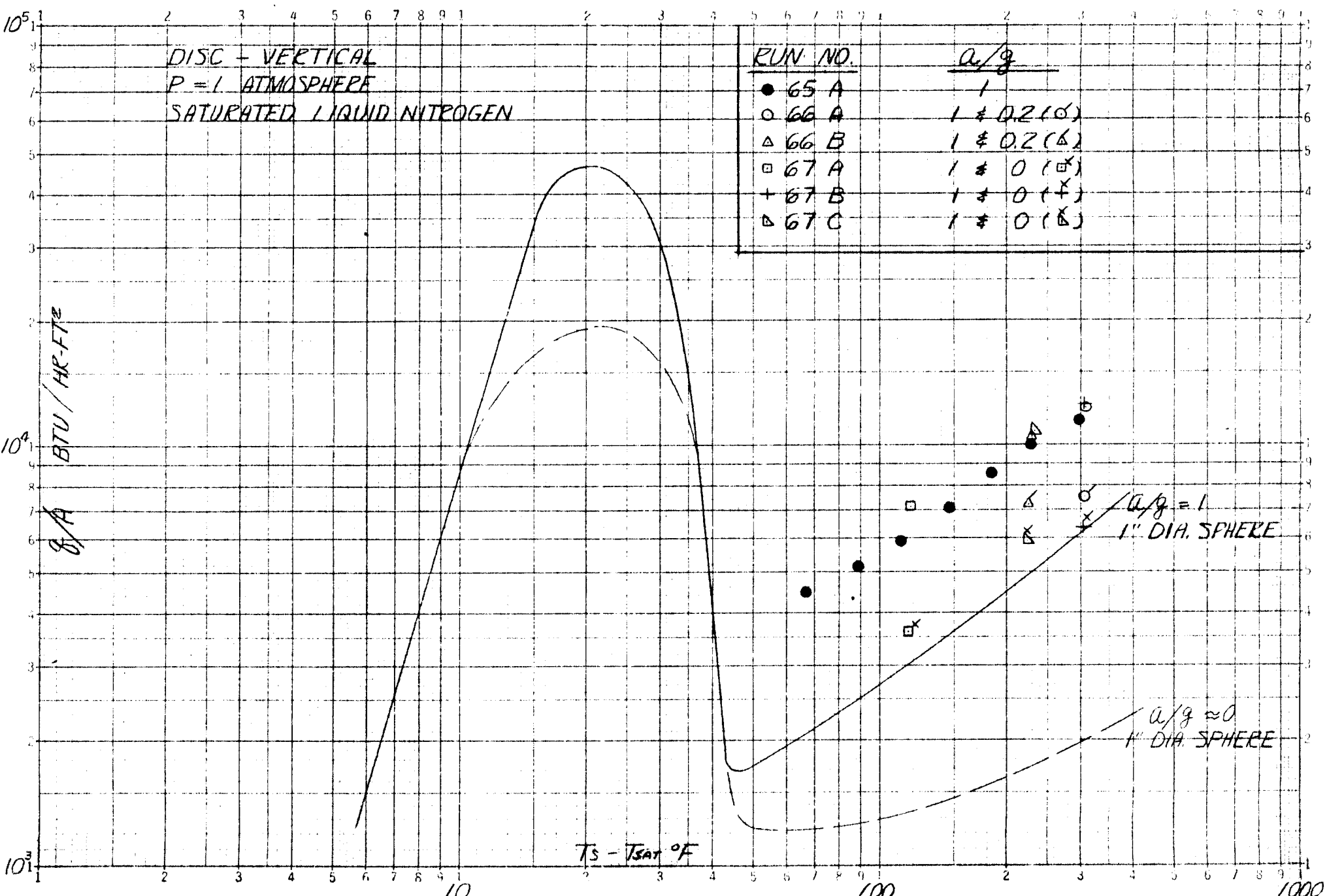


FIGURE 5. BOILING DATA WITH DISC (VERTICAL), P=1 ATM., SATURATED

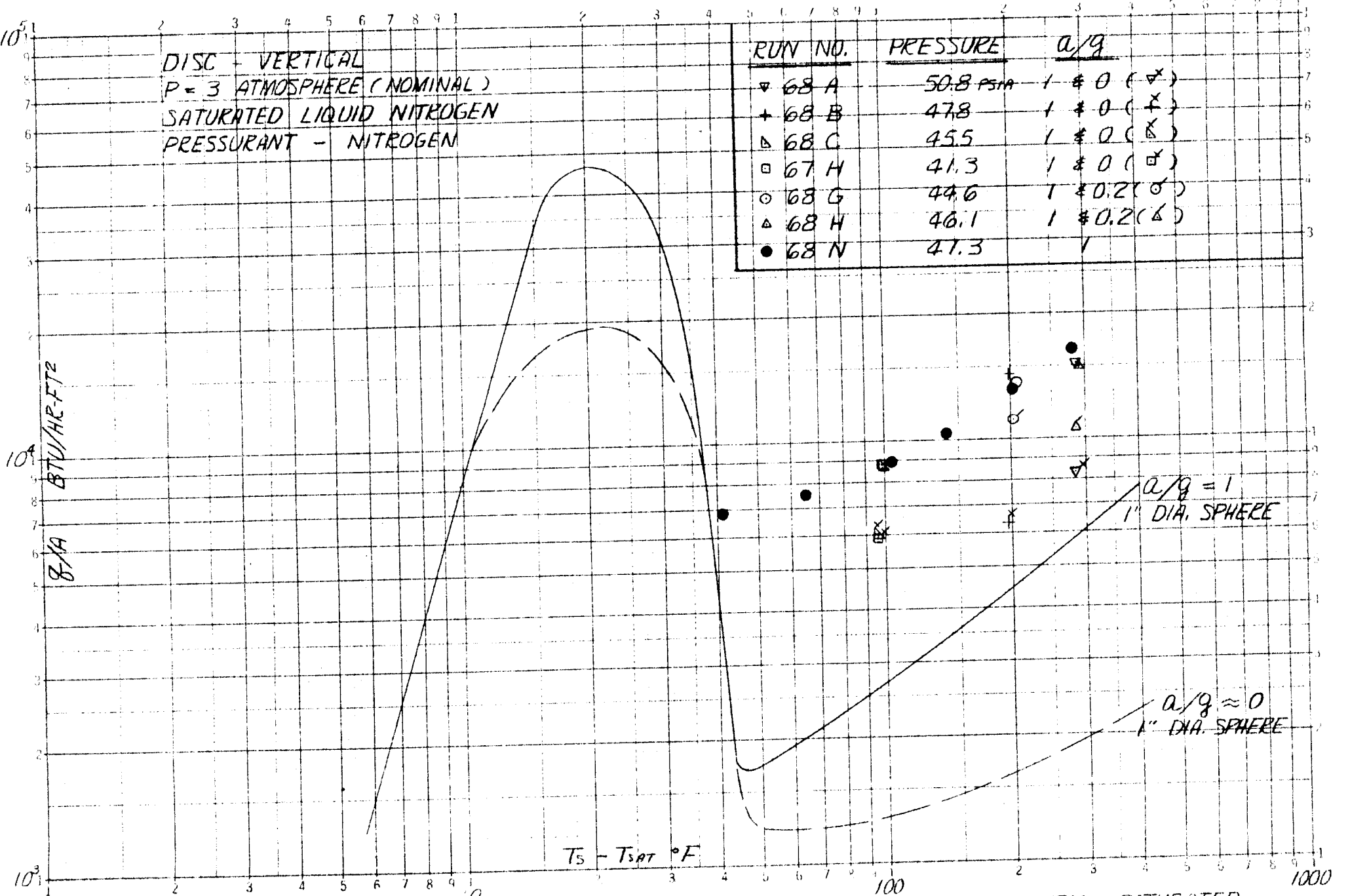


FIGURE 6. BOILING DATA WITH DISC (VERTICAL), P = 3 ATM., SATURATED

DISC - VERTICAL
 P = 3 ATMOSPHERE (NOMINAL)
 SUBCOOLED LIQUID NITROGEN
 PRESSURANT - HELIUM

RUN NO.	PRESSURE	SUBCOOLING	a/g
● 65 B	44.3 PSIA	12 - 1°F	1
○ 66 D	42.9	11	1 * 0.2 (6)
△ 66 E	44.3	6	1 * 0.2 (6)
□ 66 I	45.7	3	1 * 0.2 (6)
▽ 67 G	42.8	9	1 * 0 (8)
▽ 67 I	46.3	12	1 * 0 (8)

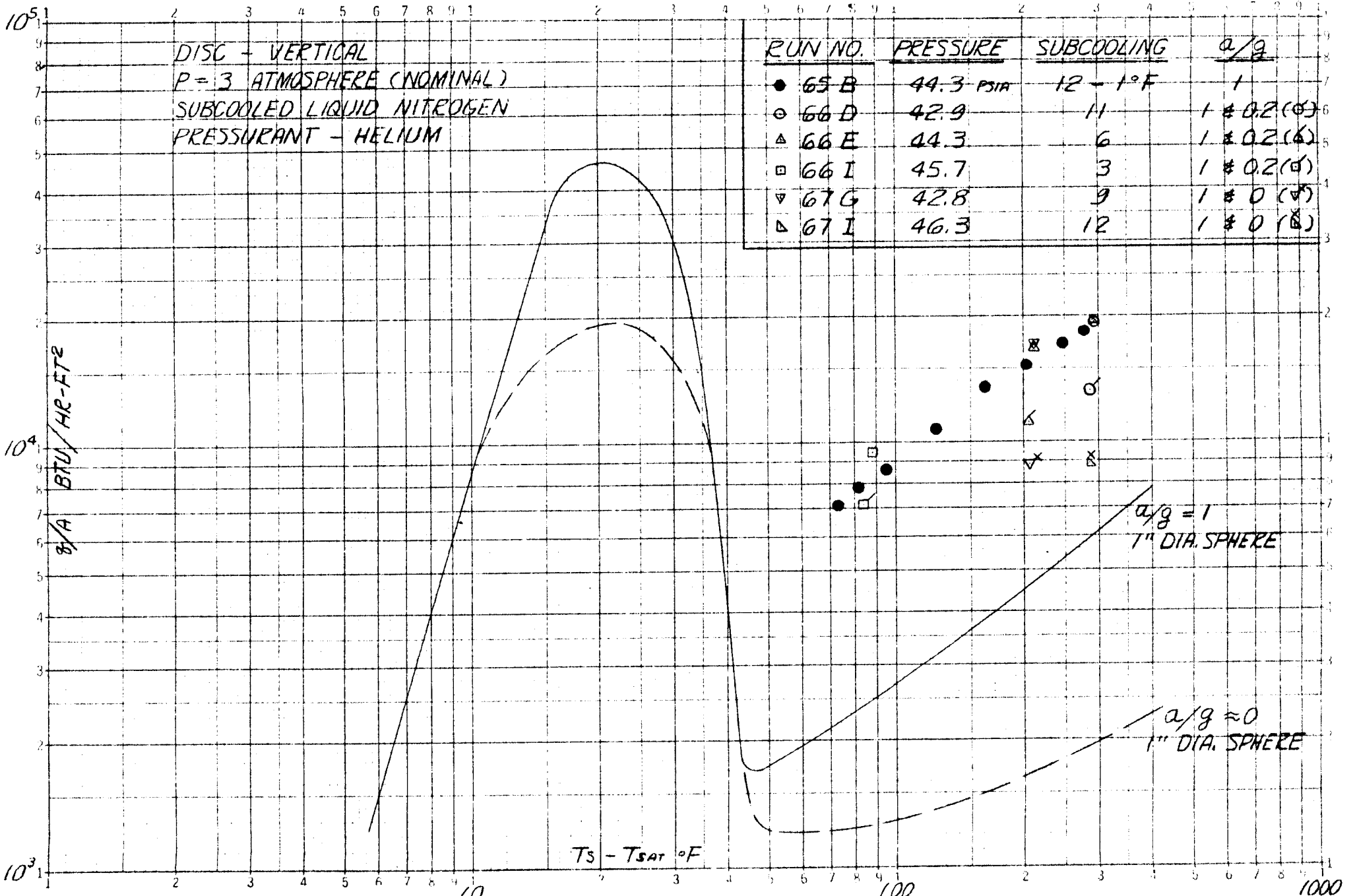


FIGURE 1. BOILING DATA WITH DISC (VERTICAL), P = 3 ATM., SUBCOOLED

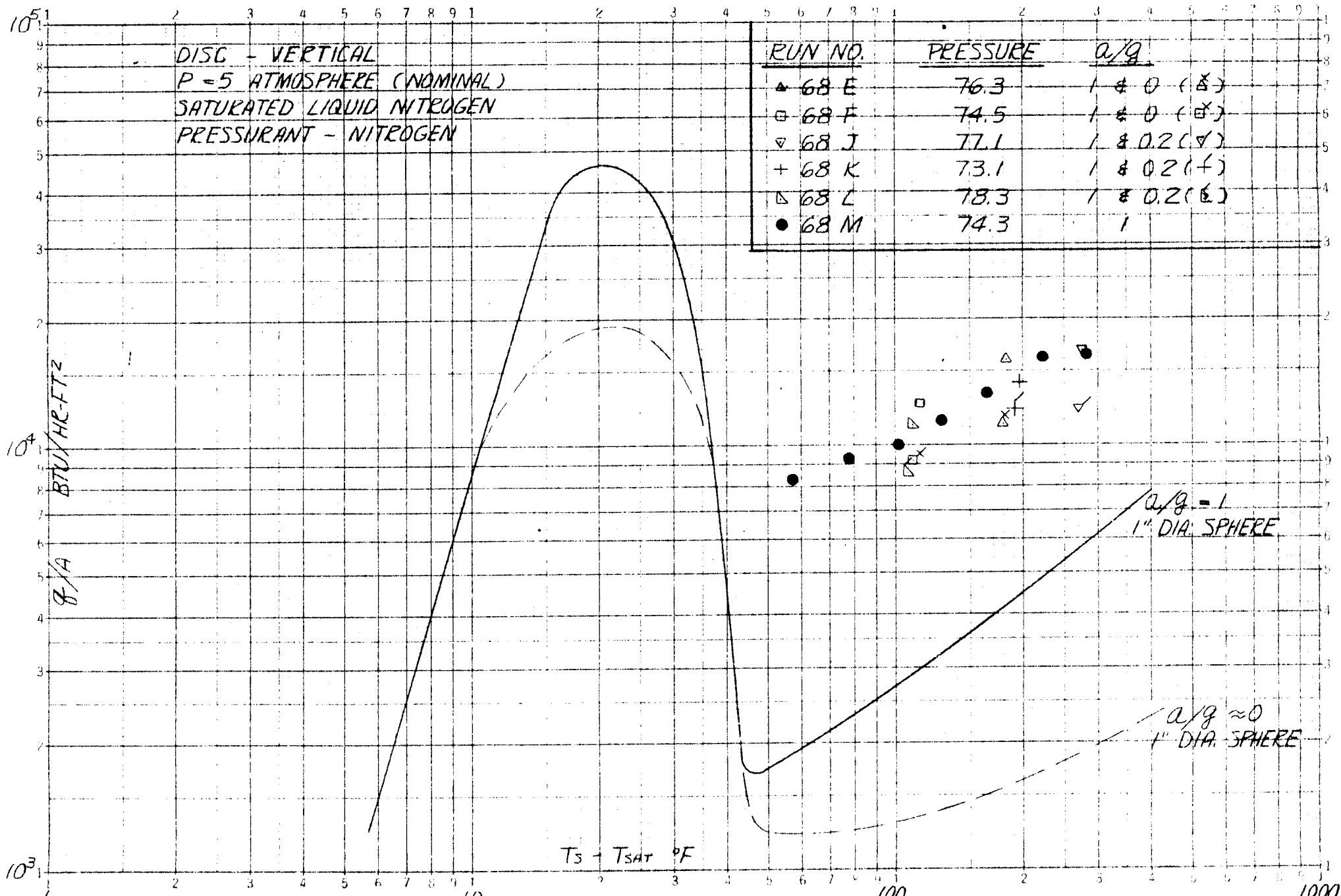


FIGURE 8. BOILING DATA WITH DISC (VERTICAL), P=5 ATM., SATURATED

DISC - VERTICAL
 P = 5 ATMOSPHERE (NOMINAL)
 SUBCOOLED LIQUID NITROGEN
 PRESSURANT - HELIUM

RUN NO	PRESSURE	SUBCOOLING	Q/G
• 65 C	74.3	18-2°F	1
○ 66 F	70.9	19	1.02 (○)
△ 66 G	73.4	20	1.02 (△)
□ 66 H	74.4	11	1.02 (□)
▽ 67 D	75.3	20	1.0 (▽)
+ 67 E	75.3	9	1.0 (+)
▷ 67 F	79.3	17	1.0 (▷)

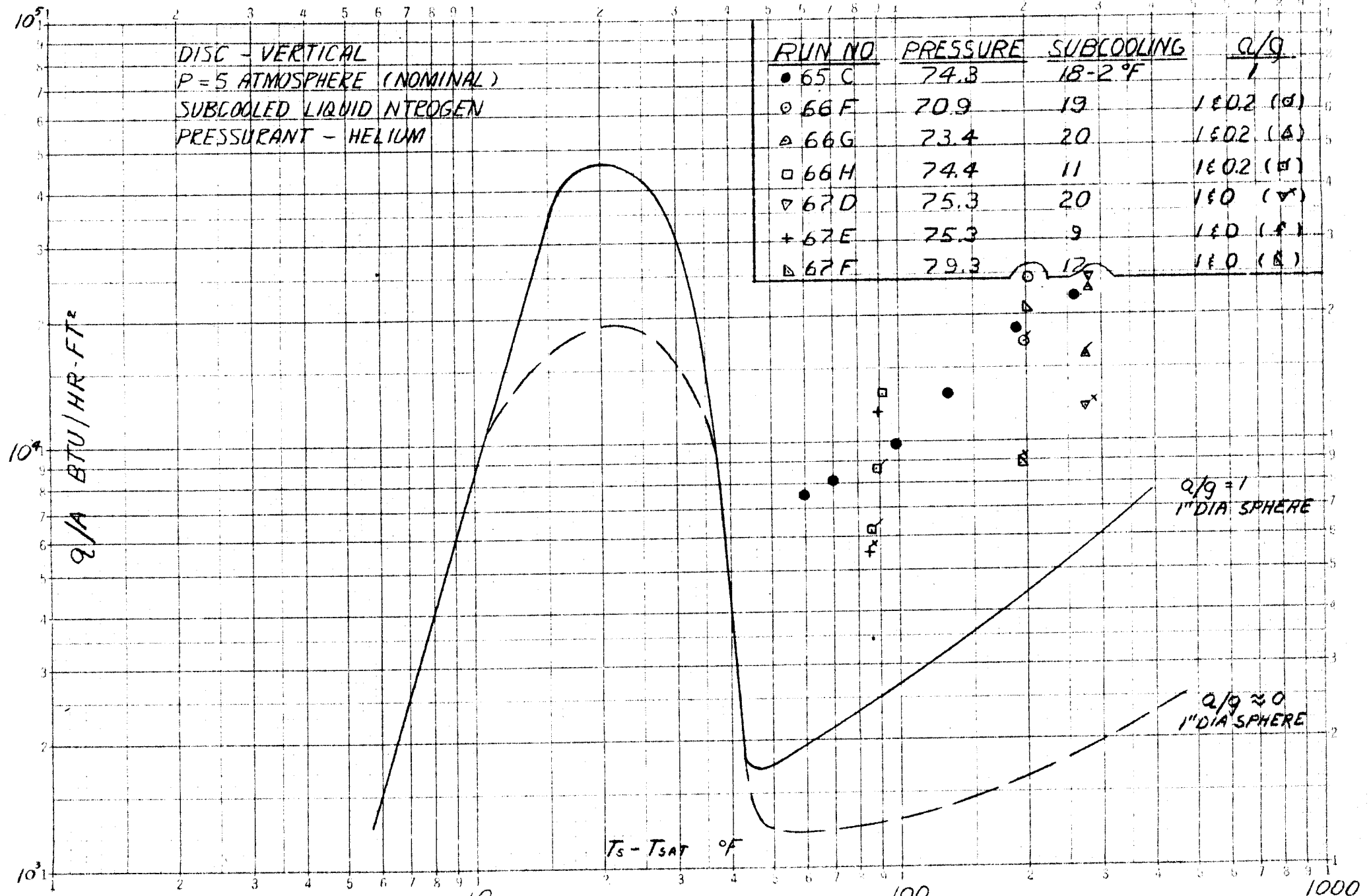


FIGURE 9. ¹⁰ BOILING DATA WITH DISC (VERTICAL), P = 5 ATM, SUBCOOLED ¹⁰⁰⁰

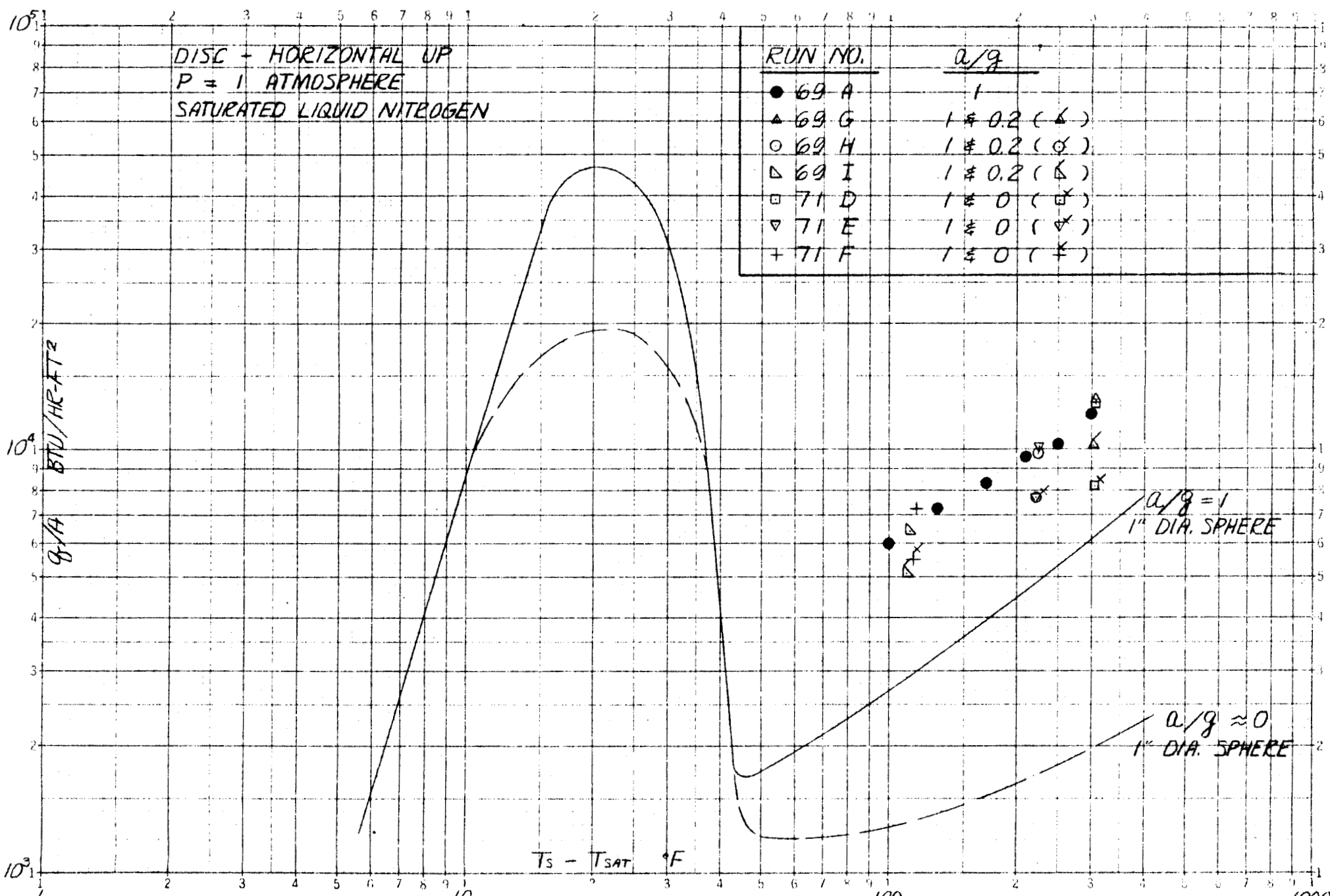


FIGURE 10. BOILING DATA WITH DISC (HORIZONTAL UP), P=1 ATM., SATURATED

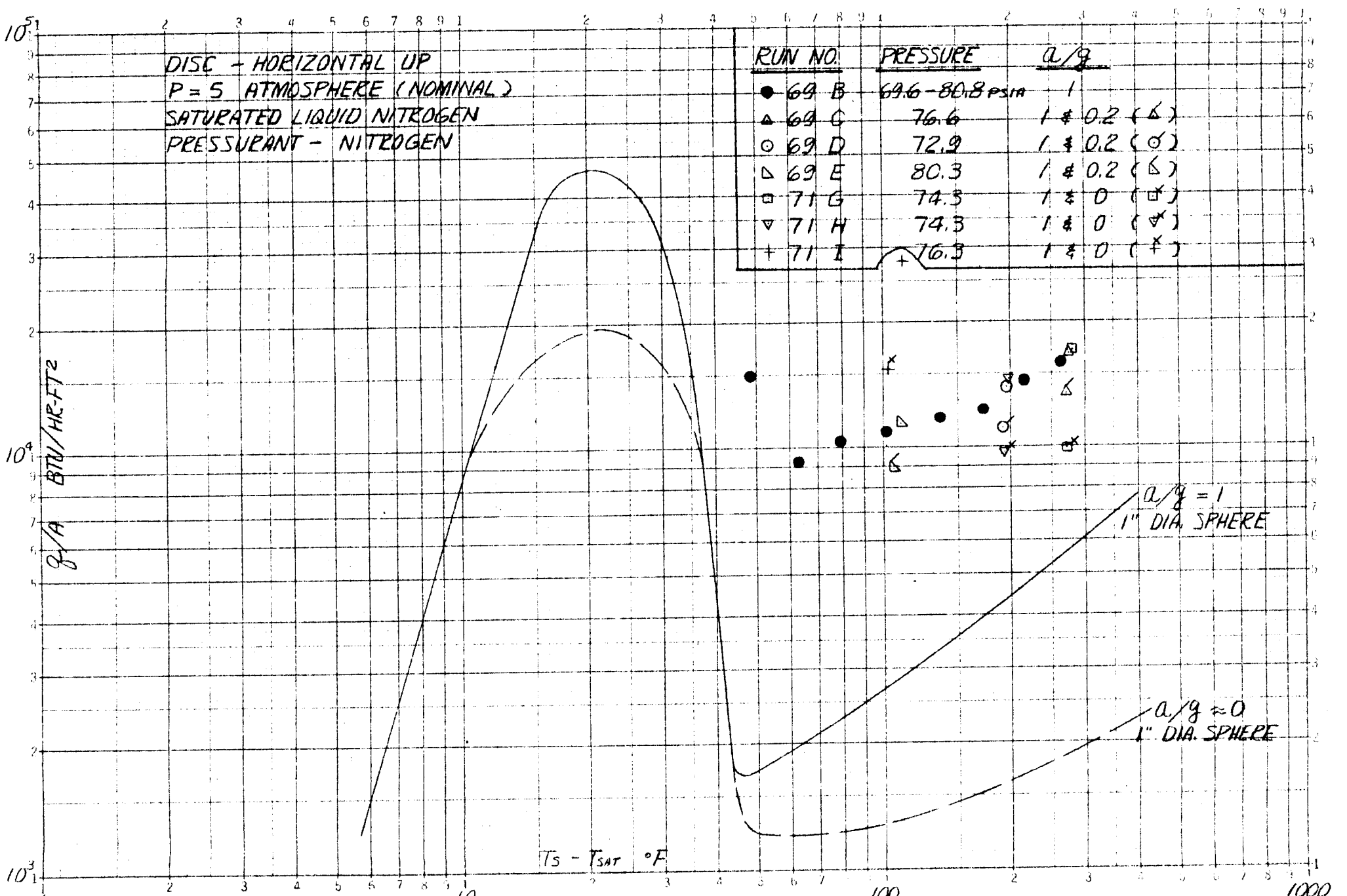
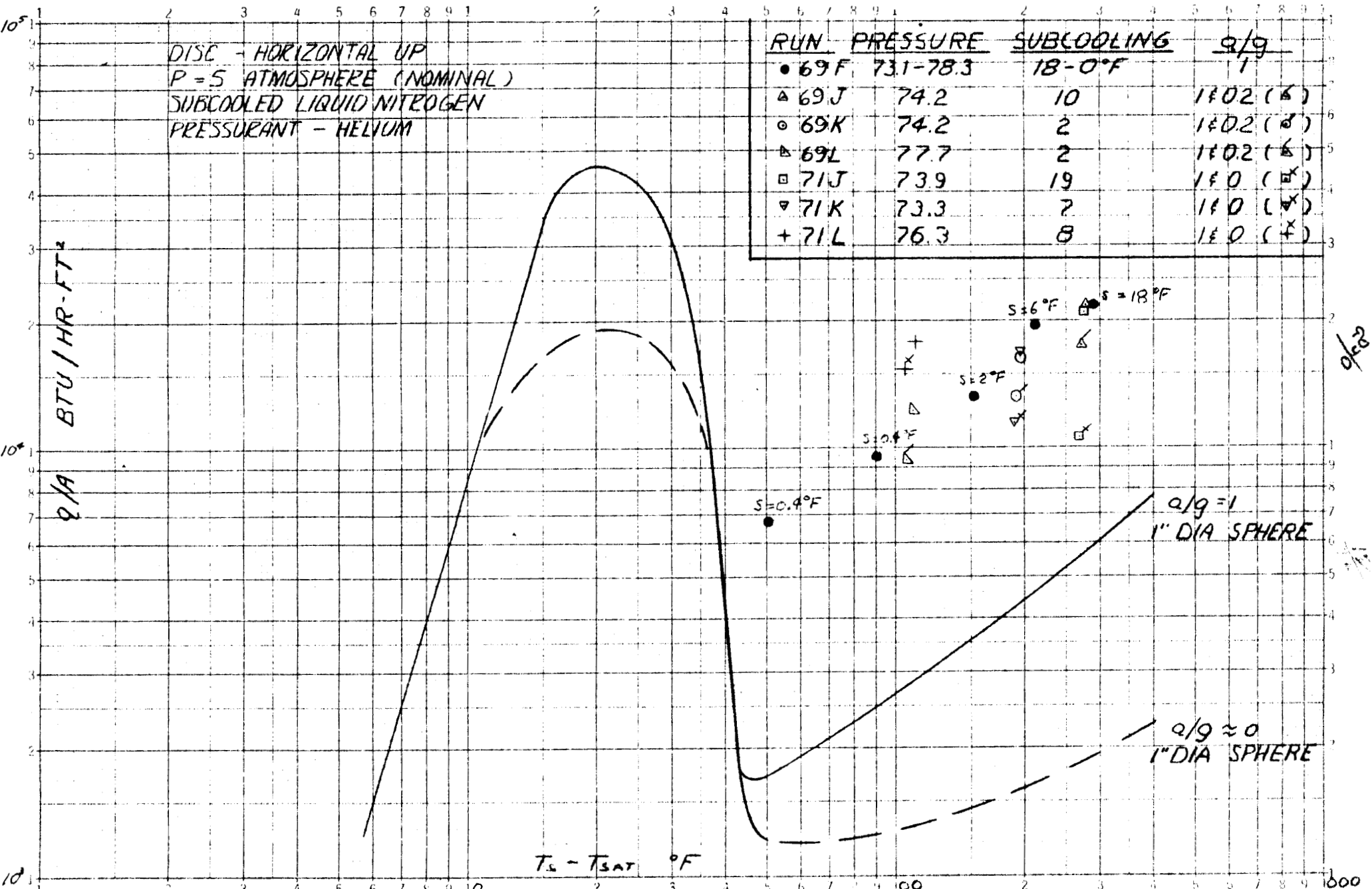


FIGURE 11. BOILING DATA WITH DISC (HORIZONTAL UP), P=5 ATM., SATURATED



DISC - HORIZONTAL UP
 P = 5 ATMOSPHERE (NOMINAL)
 SUBCOOLED LIQUID NITROGEN
 PRESSURANT - HELIUM

RUN	PRESSURE	SUBCOOLING	q/g
• 69F	73.1-78.3	18-0°F	1
△ 69J	74.2	10	140.2 (△)
○ 69K	74.2	2	140.2 (○)
△ 69L	77.7	2	140.2 (△)
□ 71J	73.9	19	140 (□)
▽ 71K	73.3	7	140 (▽)
+ 71L	76.3	8	140 (+)

FIGURE 12. BOILING DATA WITH DISC (HORIZONTAL UP), P=5ATM, SUBCOOLED

DISC - HORIZONTAL DOWN
P = 1 ATMOSPHERE
SATURATED LIQUID NITROGEN

RUN NO.	a/g
● 70 A	1
□ 70 G	1 ≠ 0.2 (□)
○ 70 H	1 ≠ 0.2 (○)
△ 70 I	1 ≠ 0.2 (△)
△ 71 A	1 ≠ 0 (△)
▽ 71 B	1 ≠ 0 (▽)
+ 71 C	1 ≠ 0 (+)

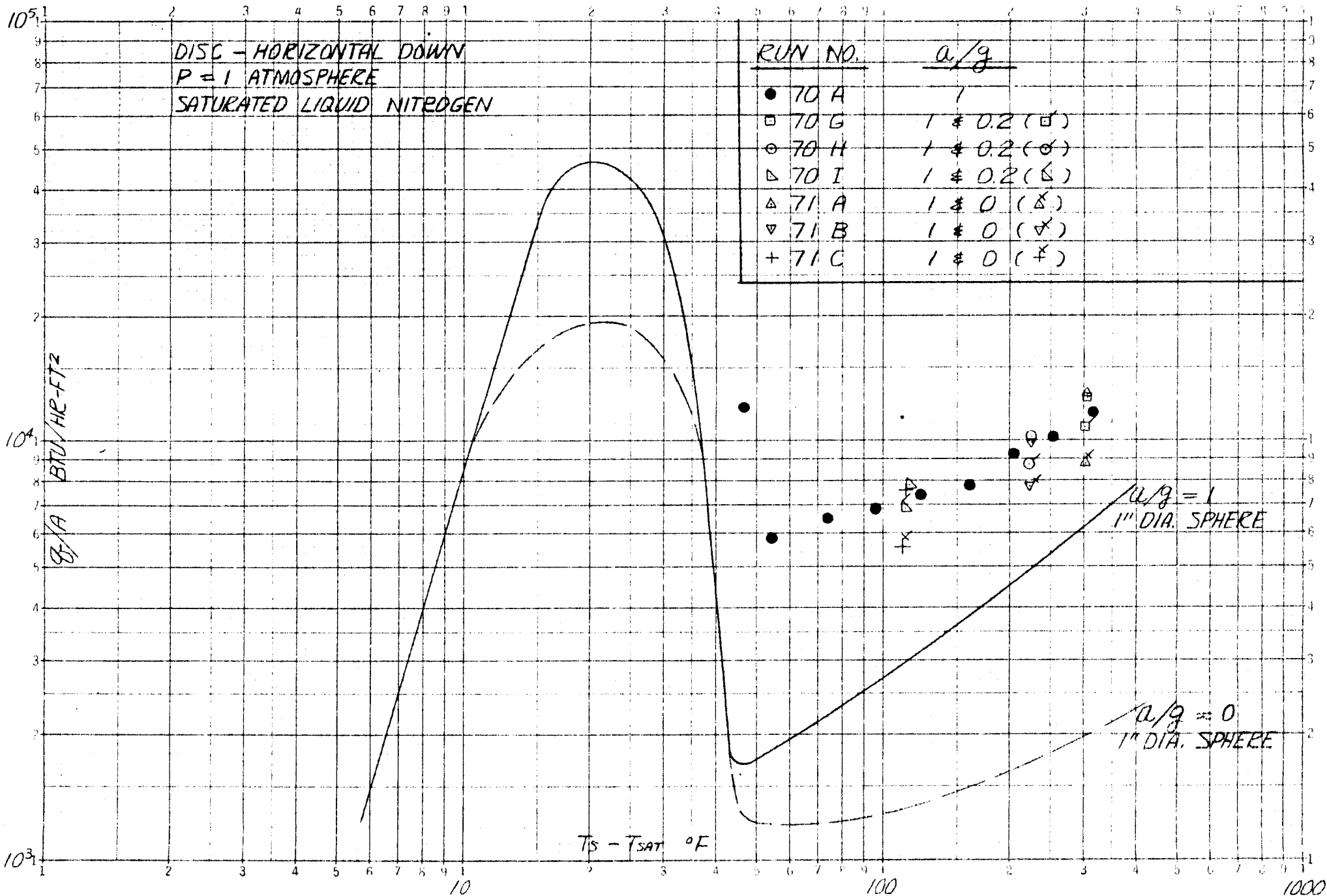


FIGURE 13. BOILING DATA WITH DISC (HORIZONTAL DOWN), P = 1 ATM., SATURATED

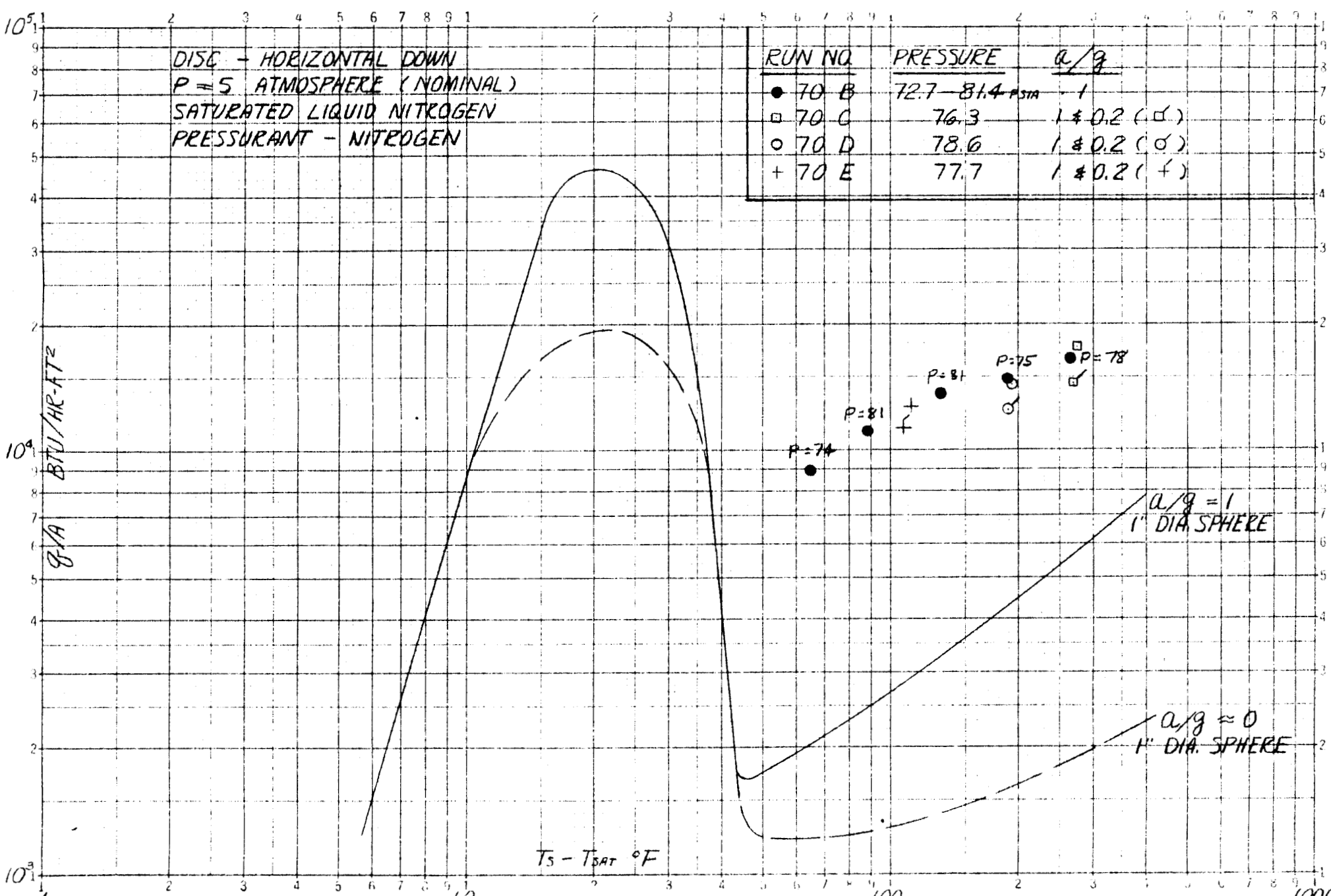


FIGURE 14. BOILING DATA WITH DISC (HORIZONTAL DOWN), P=5 ATM., SATURATED

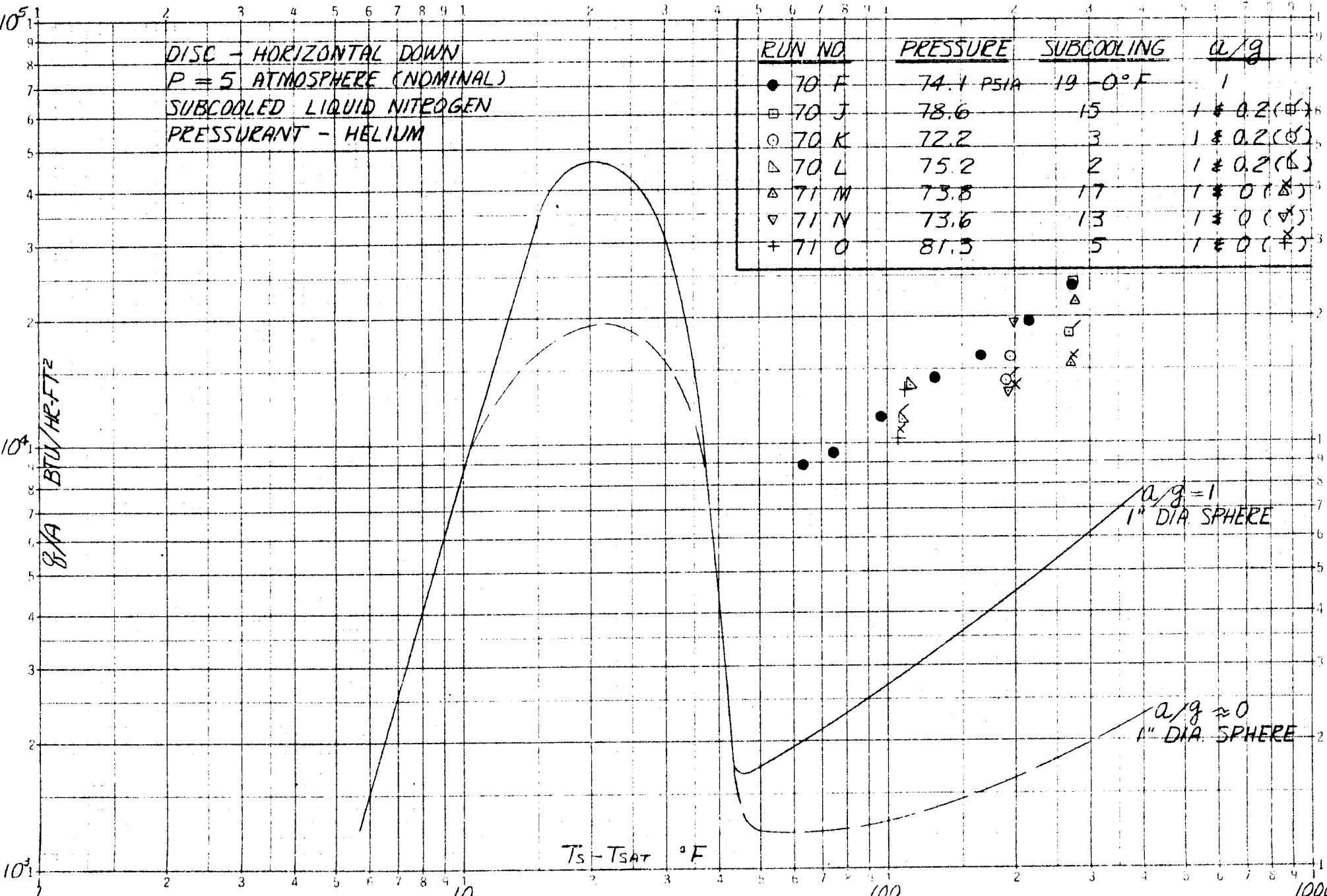
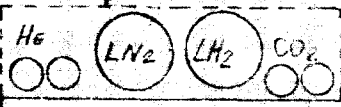


FIGURE 15. ELING DATA WITH DISC (HORIZONTAL DOWN), P = 5 ATM, SUBCOOLED

ELEVATOR

STEEL SHEET OVER FOR ROLLING COIL

WIRE CAGE

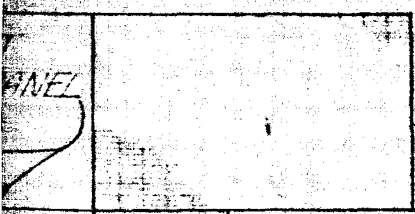


AIR LOCK ROOM

SHAFT CHAMBER

5750000 V. 5

6
93

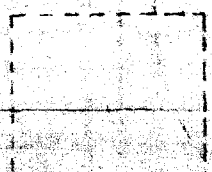


PARTS
DRAWER

HOIST UNIT

BEAM IN PIT

GASOLINE
FLOOR



2

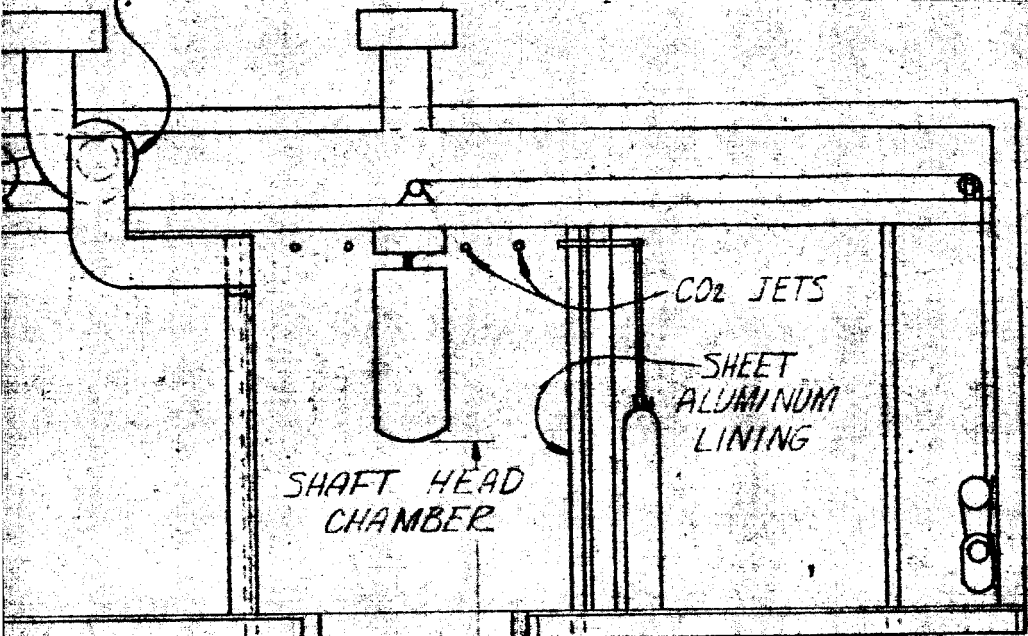
ELEVATOR TOWER

DOOR
TO
STAIR

VENT

AT FIRST
LEVEL

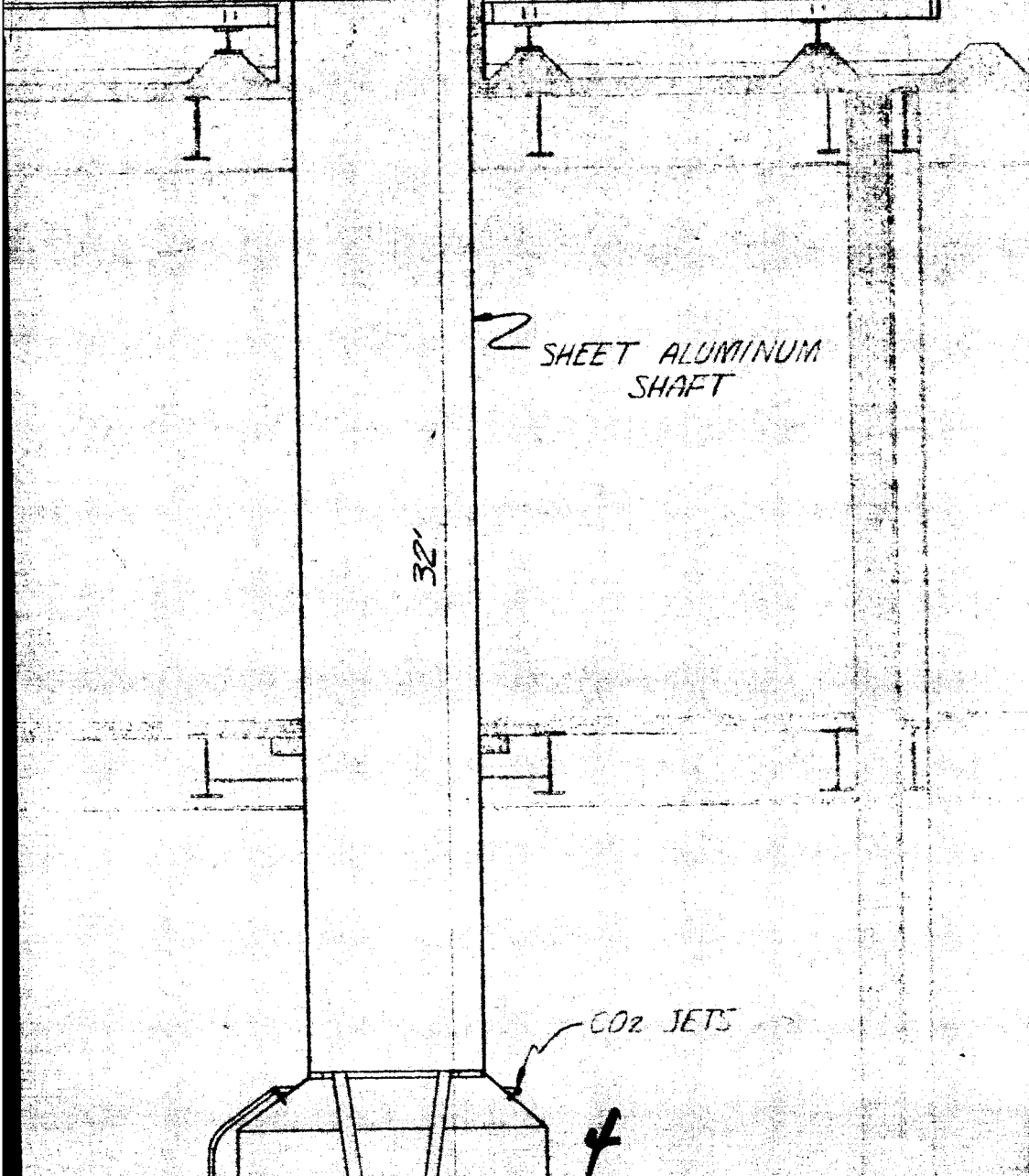
EXHAUST FAN



SHAFT HEAD CHAMBER

CO2 JETS

SHEET ALUMINUM LINING



SHEET ALUMINUM SHAFT

32'

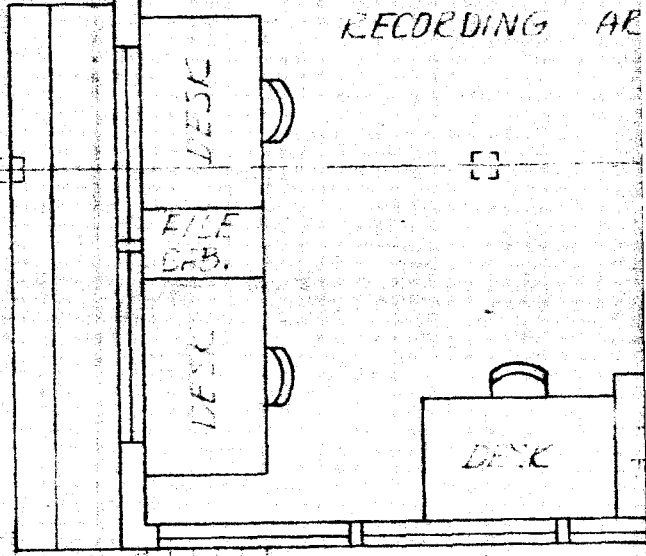
CO2 JETS

4

HEIGHT OF COOLING TOWER



CONTROL AND
RECORDING AREA



6

WORKSHOP
AREA

STAIR
CASE

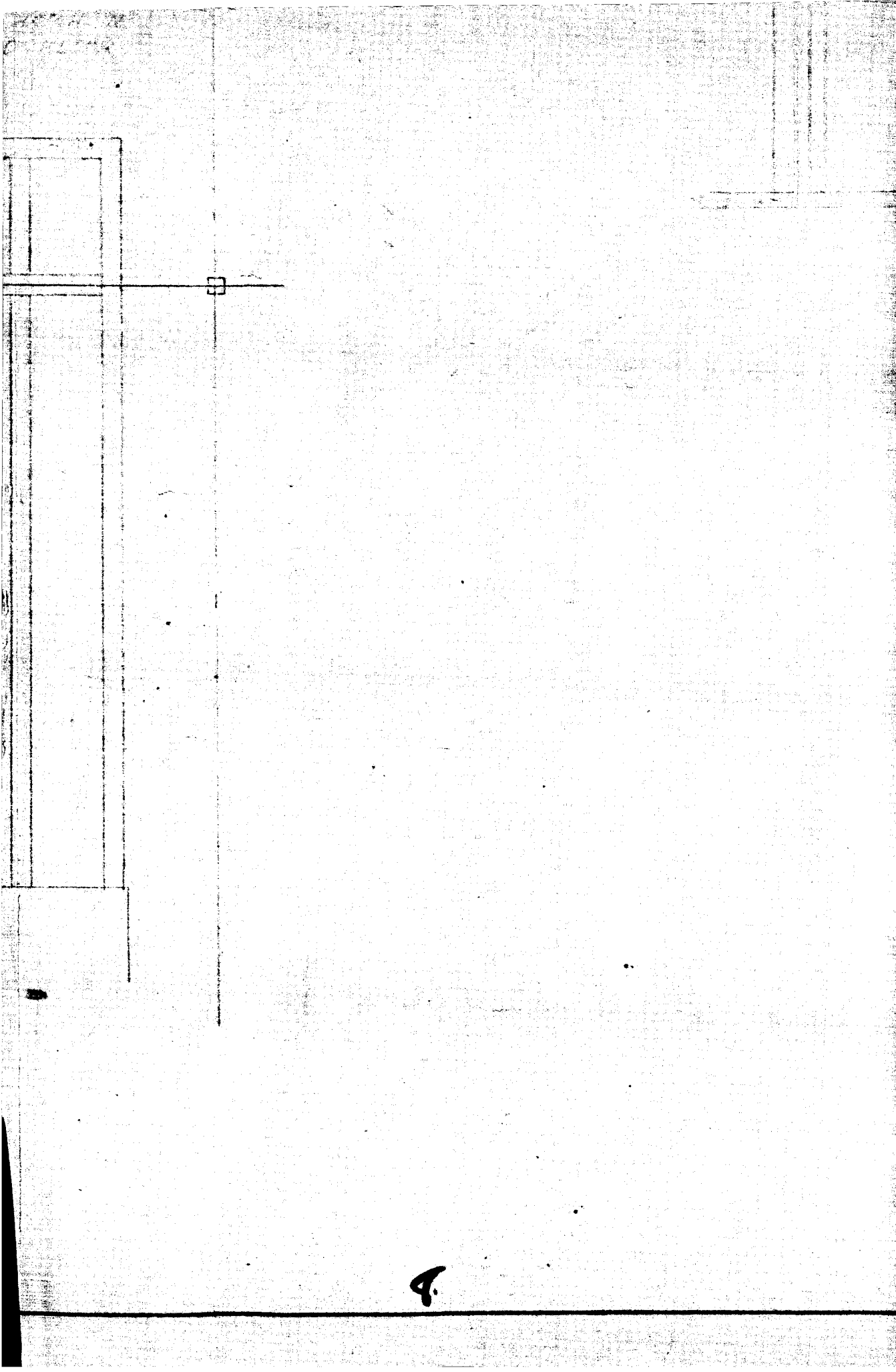
WORK BENCH

TOOL & M.T.

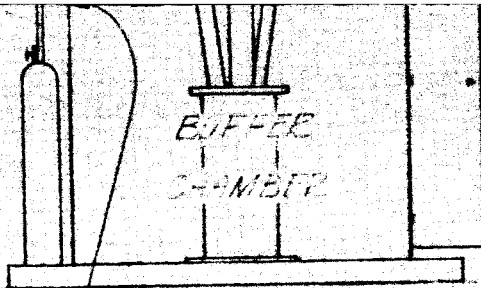
DRAWING
TABLE

COOLING TOWER

FRESH COOLING TOWER



4.



SHEET ALUMINUM

SCALE
DATE

FIGURE 16 . ZERO-GRAVITY

PROPOSED ZERO GRAVITY FACILITY
FOR LIQUID HYDROGEN -

1/4" = 1'
6-1-64

APPROVED BY

DRAWN BY BB
OEA PROJ. 04268

10

DRAWING NUMBER

LIQUID HYDROGEN RESEARCH FACILITY

EVING AND COUNTERWEIGHT EYE

DID OPERATED RELEASE YOKE

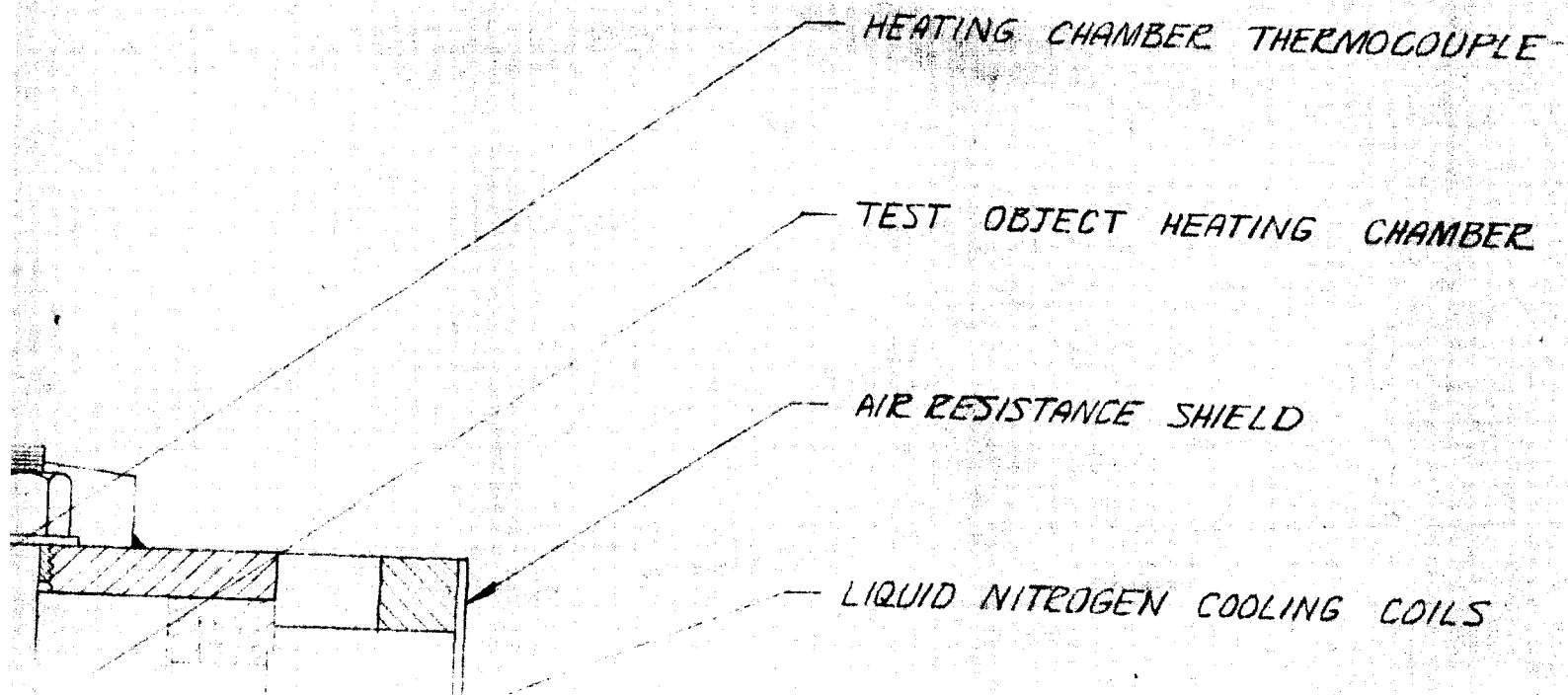
SHIELD RELEASE RING

VESSEL SUPPORT

NITROGEN FILL LINE

LEVEL INDICATOR FOR LIQUID NITROGEN

OBJECT INSERTION ROD



A hand-drawn diagram on a grid background showing a cryostat system. The diagram consists of several horizontal lines representing different layers or components. From top to bottom, the layers are: a thin top layer, a thicker layer, a layer with a central rod, a thick vacuum-insulated layer, a layer with two shields, a layer with two vent lines, and a bottom layer. Leader lines connect each label to its corresponding layer. The labels are: TEST OBJECT, RADIANT HEATER FOR TEST OBJECT, CRYOSTAT SUPPORT ROD, VACUUM INSULATED LIQUID HYDROGEN FILL LINE, RADIATION SHIELDS, HYDROGEN VENT LINE (2 REQ'D), VACUUM FITTING, and LIQUID NITROGEN. A handwritten number '3' is visible on the right side of the page.

TEST OBJECT

RADIANT HEATER FOR TEST OBJECT

CRYOSTAT SUPPORT ROD

VACUUM INSULATED LIQUID HYDROGEN FILL LINE

RADIATION SHIELDS

HYDROGEN VENT LINE (2 REQ'D)

VACUUM FITTING

LIQUID NITROGEN

A hand-drawn diagram of a cryostat cross-section. The diagram is divided into several horizontal layers. From top to bottom, the layers are: OUTER VESSEL, POWDER INSULATION, CRYOSTAT, SUPER INSULATION, LIQUID LEVEL DETECTORS, and INERT GAS SPACE. A vertical line on the left side represents the central axis. A jagged crack is drawn in the powder insulation layer. A handwritten number '4' is located on the right side of the diagram.

OUTER VESSEL

POWDER INSULATION

CRYOSTAT

SUPER INSULATION

LIQUID LEVEL DETECTORS

INERT GAS SPACE

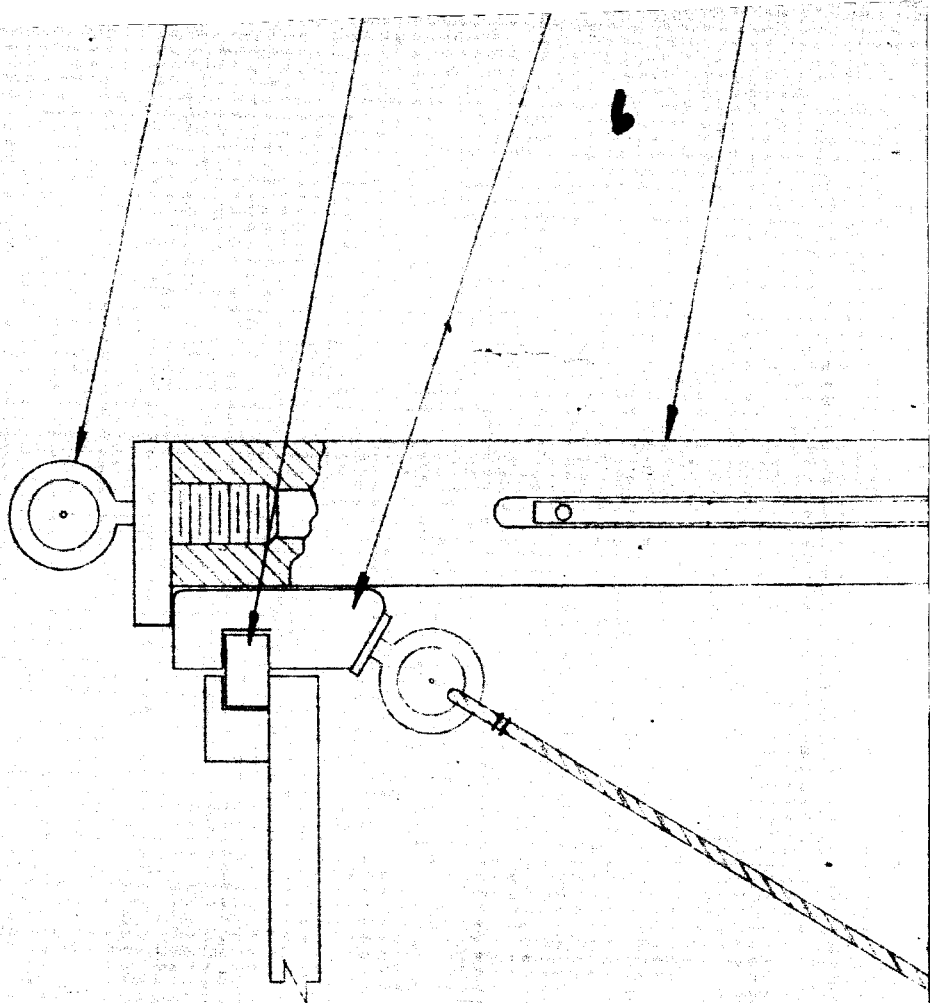
4

BULK LIQUID THERMOCOUPLE PROBES

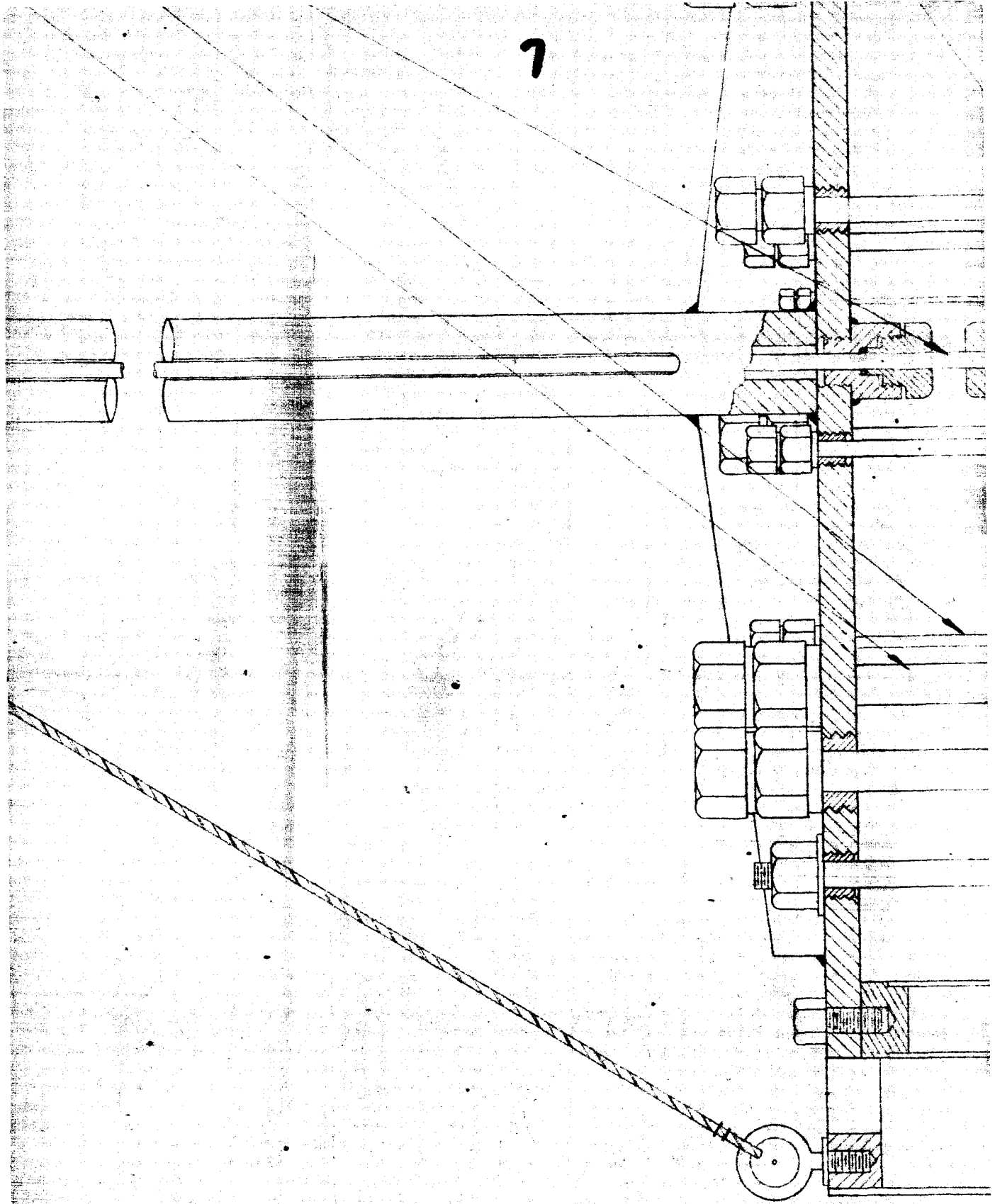
LIQUID HYDROGEN

TEST OBJECT IN IMMERSSED POSITION

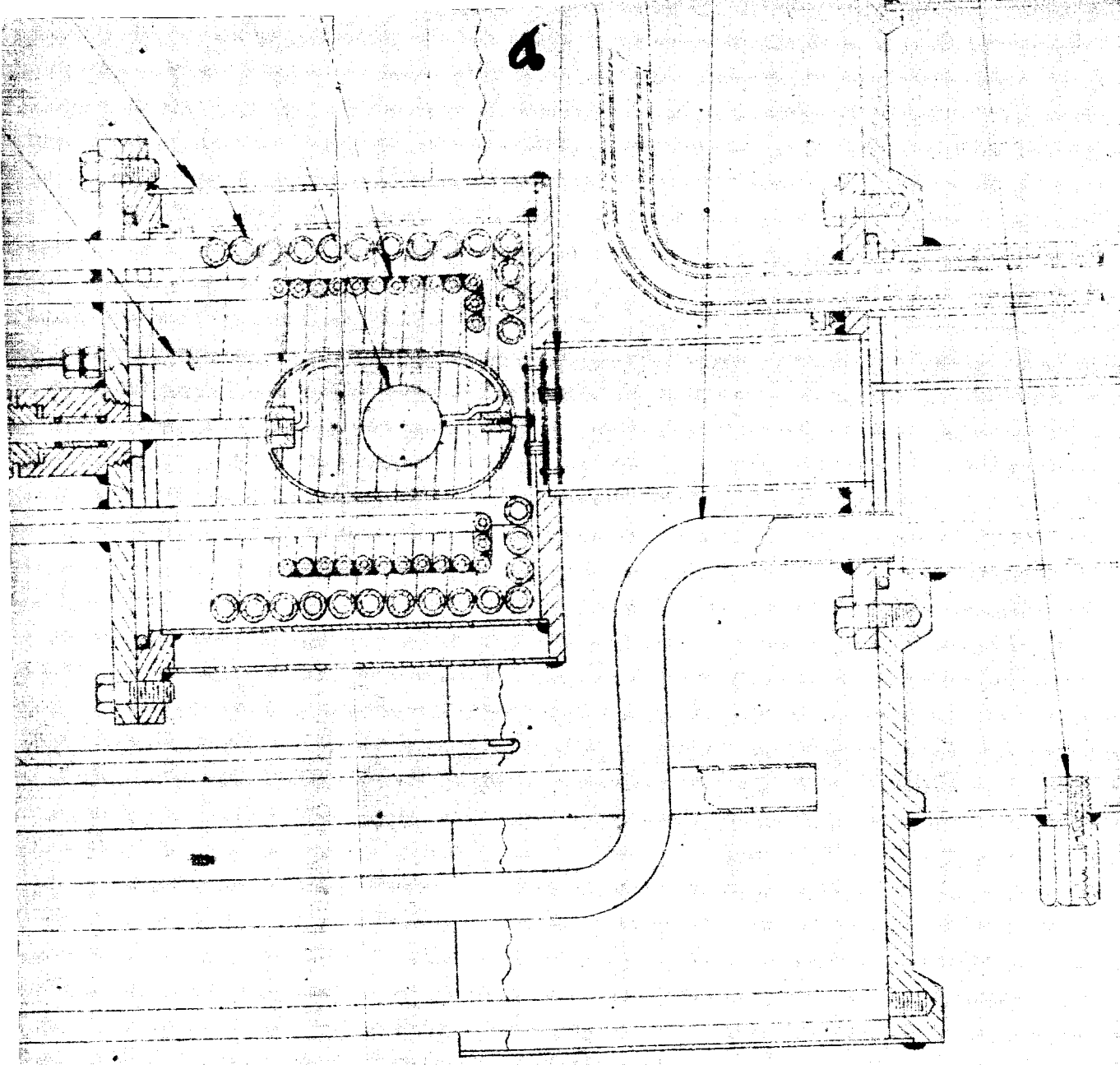
9



7



6



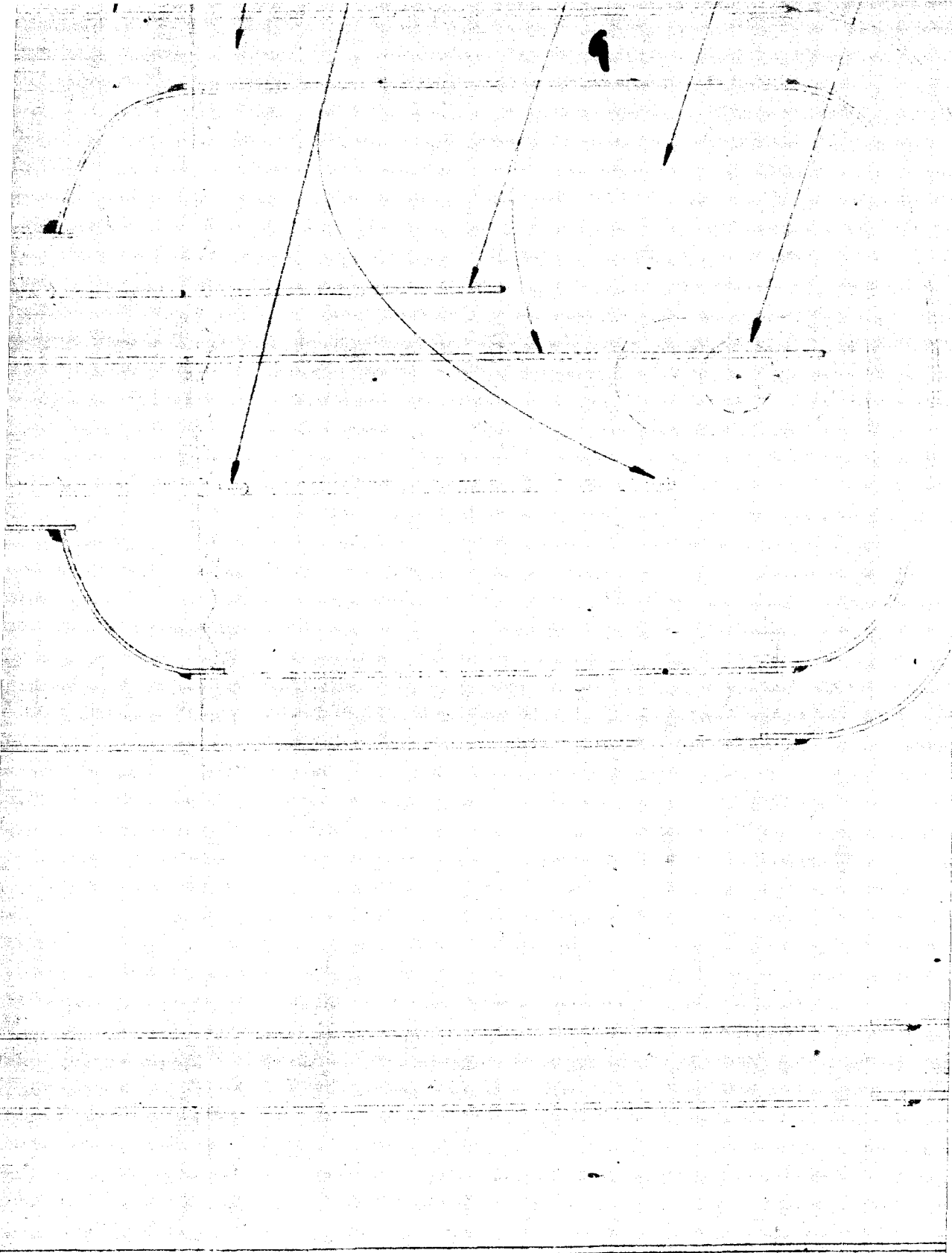


FIGURE 17

• LIQUID HYDROGEN
TEST PACKAGE AS

10

ZERO-GRAVITY
SEMBLY

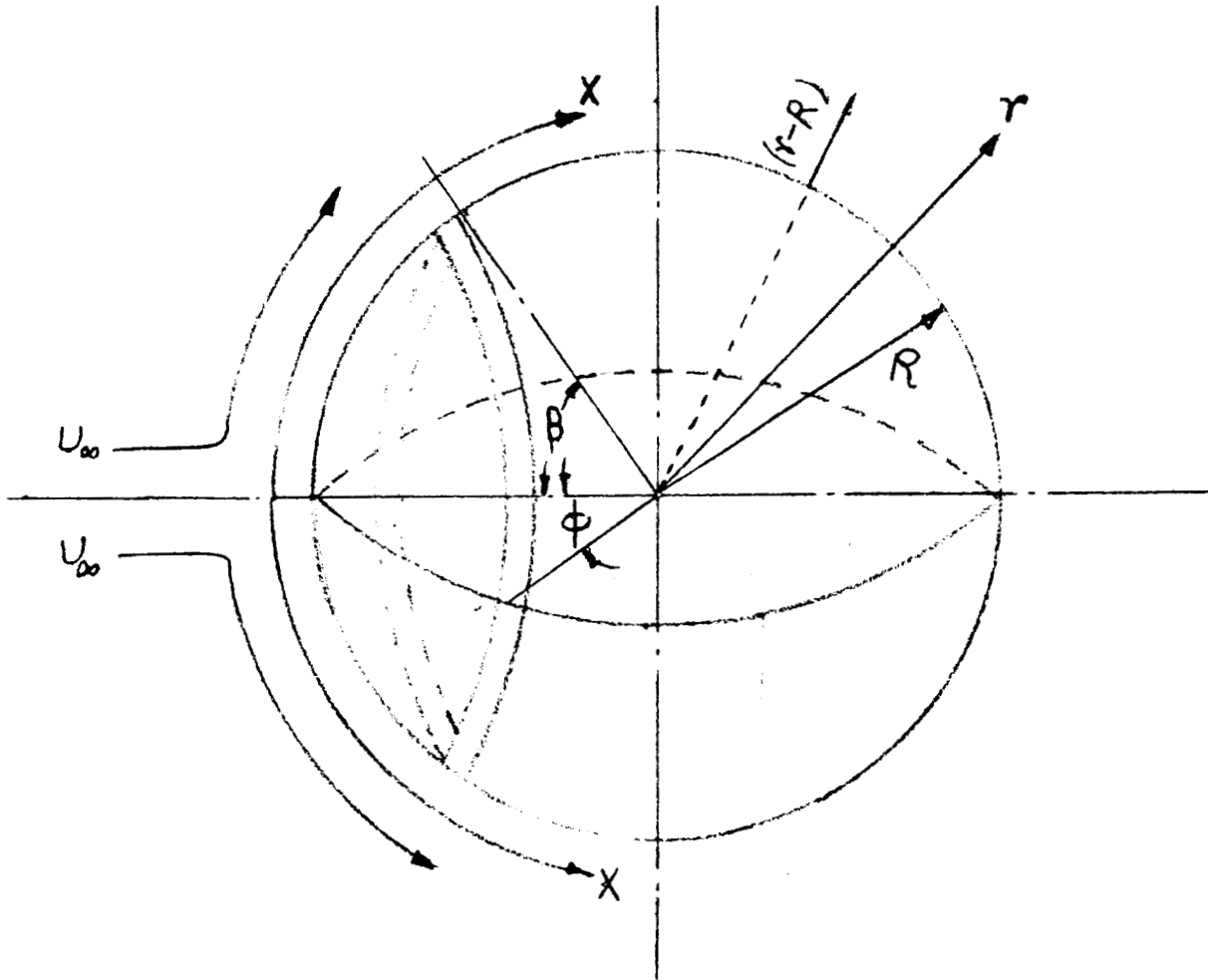


Fig. 18 FLOW ABOUT A SPHERICAL BUBBLE

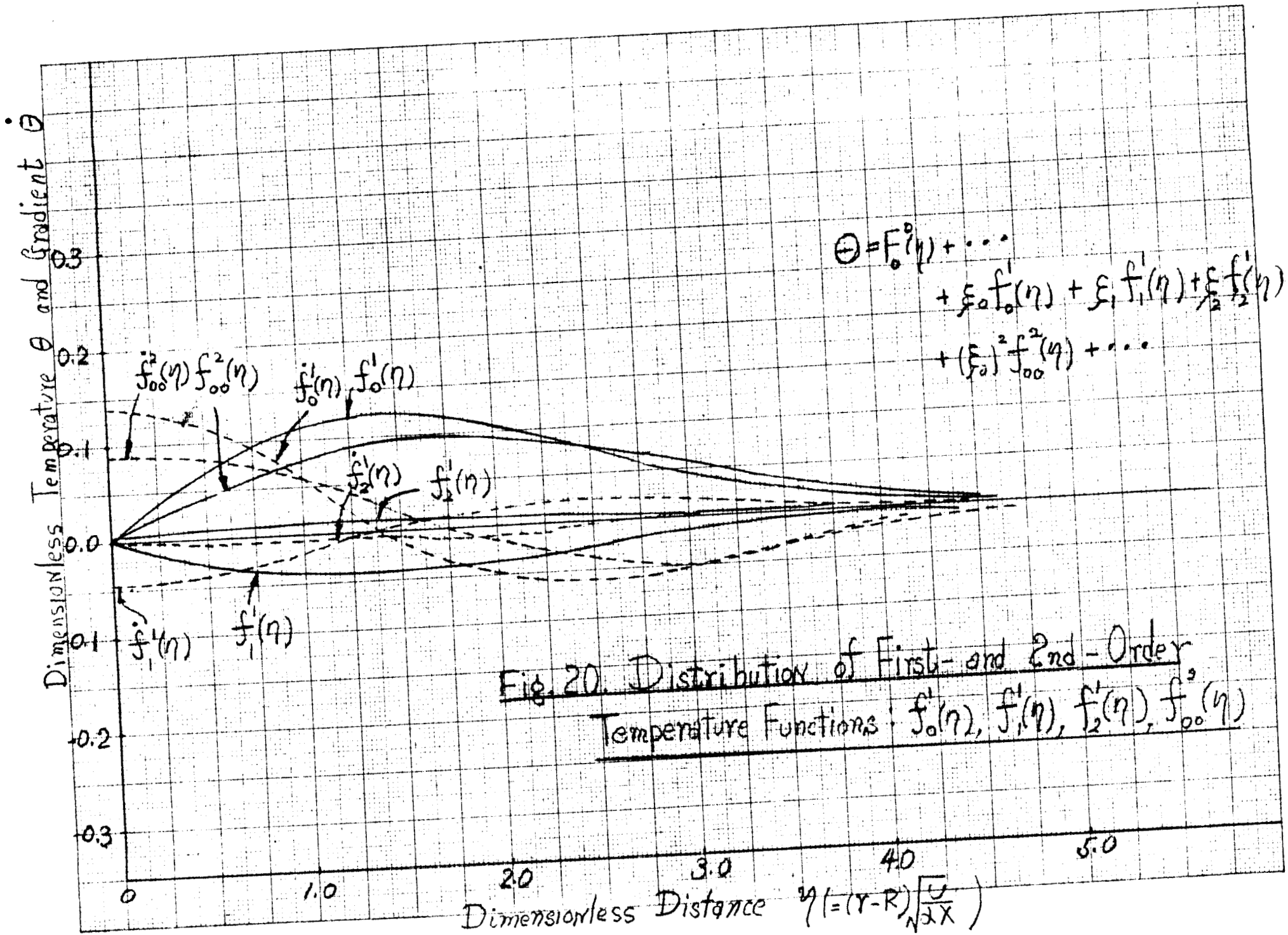
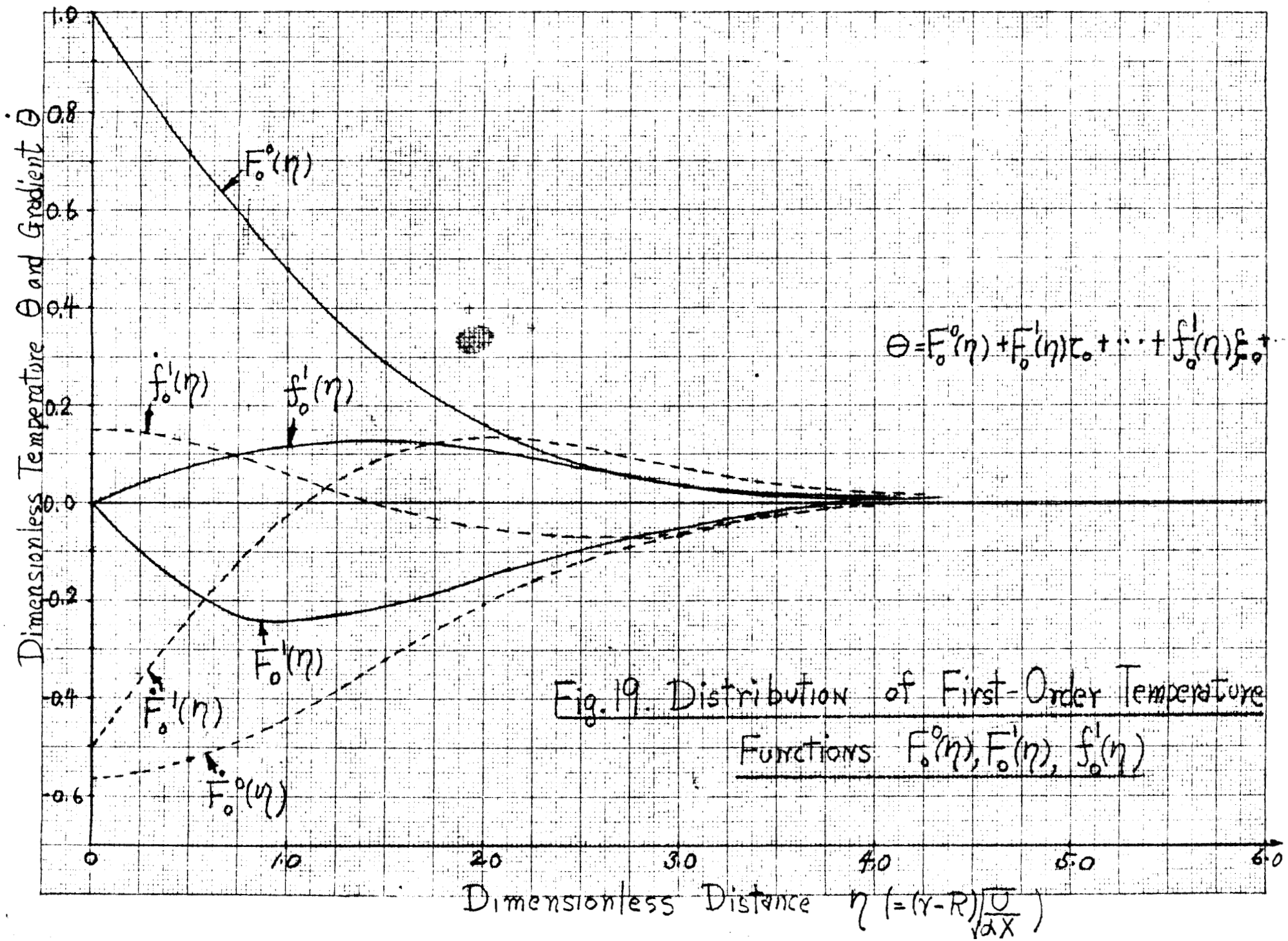


Fig. 20. Distribution of First- and 2nd-Order Temperature Functions: $f_0^1(\eta)$, $f_1^1(\eta)$, $f_2^1(\eta)$, $f_{00}^2(\eta)$



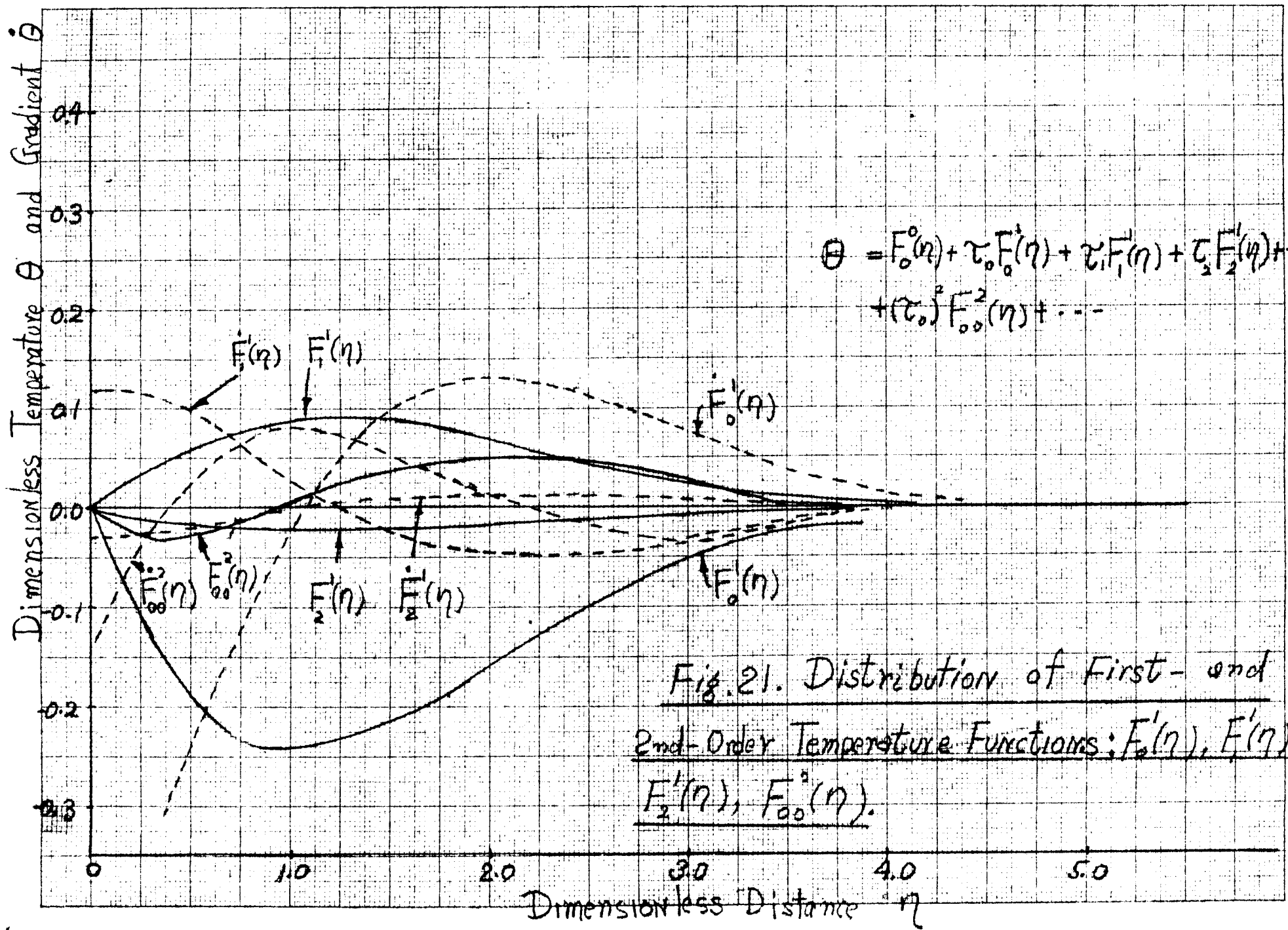


Fig. 22. BUBBLE GROWTH

Quasi-Steady Case

- 2nd-Order, 1st-Power Sol.
 - x 1st-Order, 1st-Power Sol.
 - o 1st-Order, 2nd-Power Sol.
 - 0th Order, 1st-Power Sol.
 - Δ- Longer Acc. 2nd Order
- Pecklet $NO = 300$.

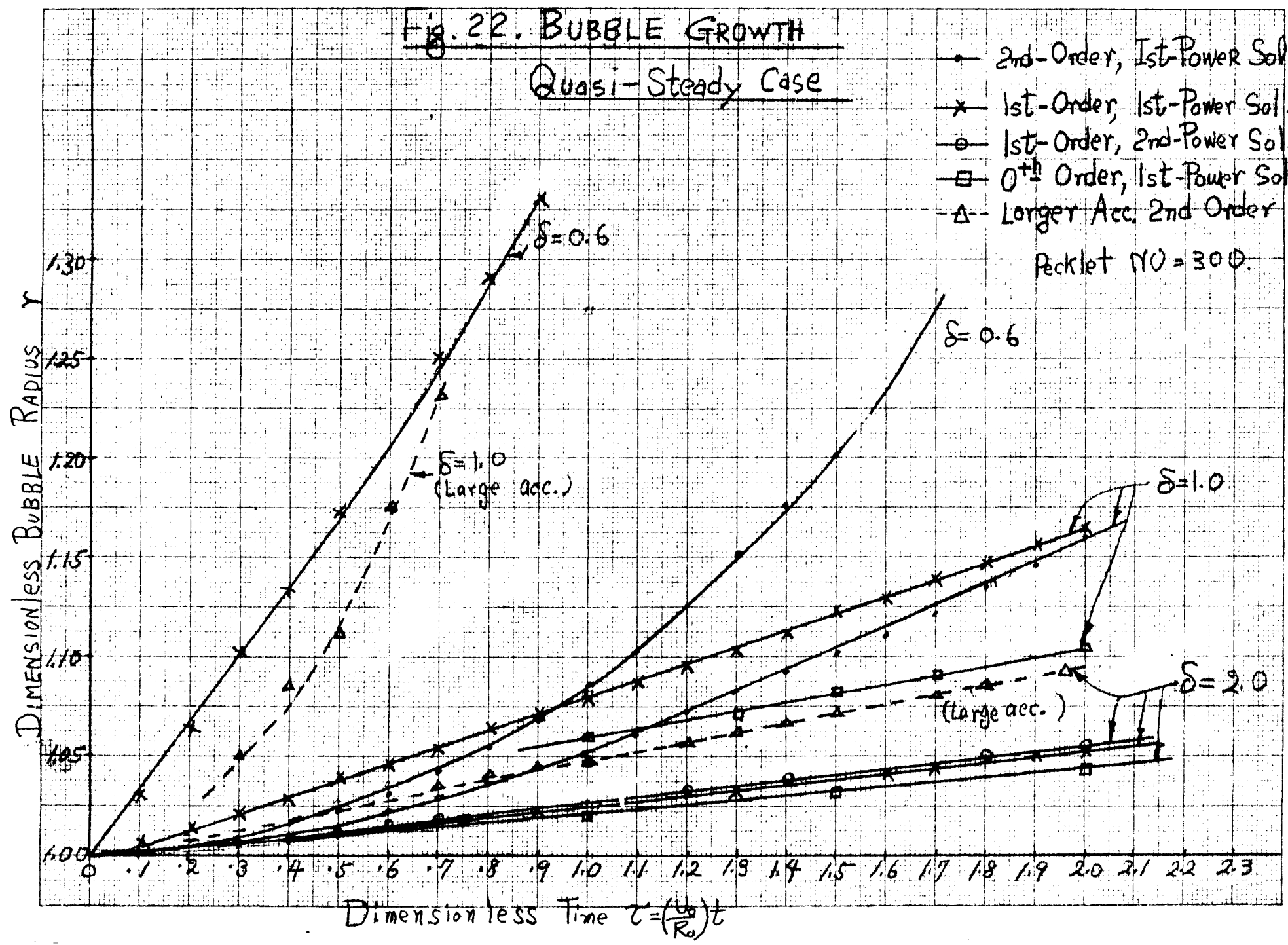


Fig. 23. BUBBLE GROWTH SPEED

Quasi-Steady Case

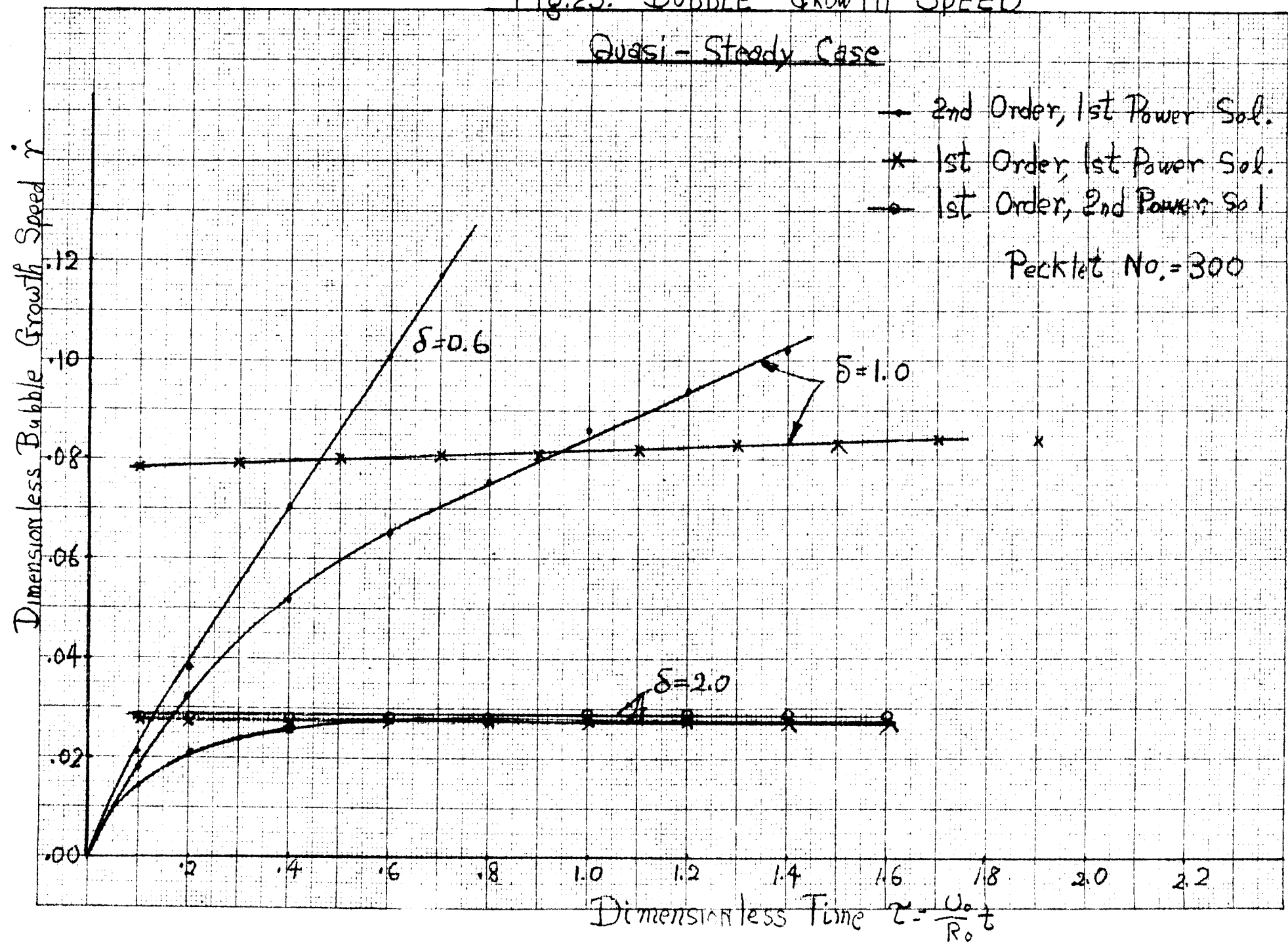
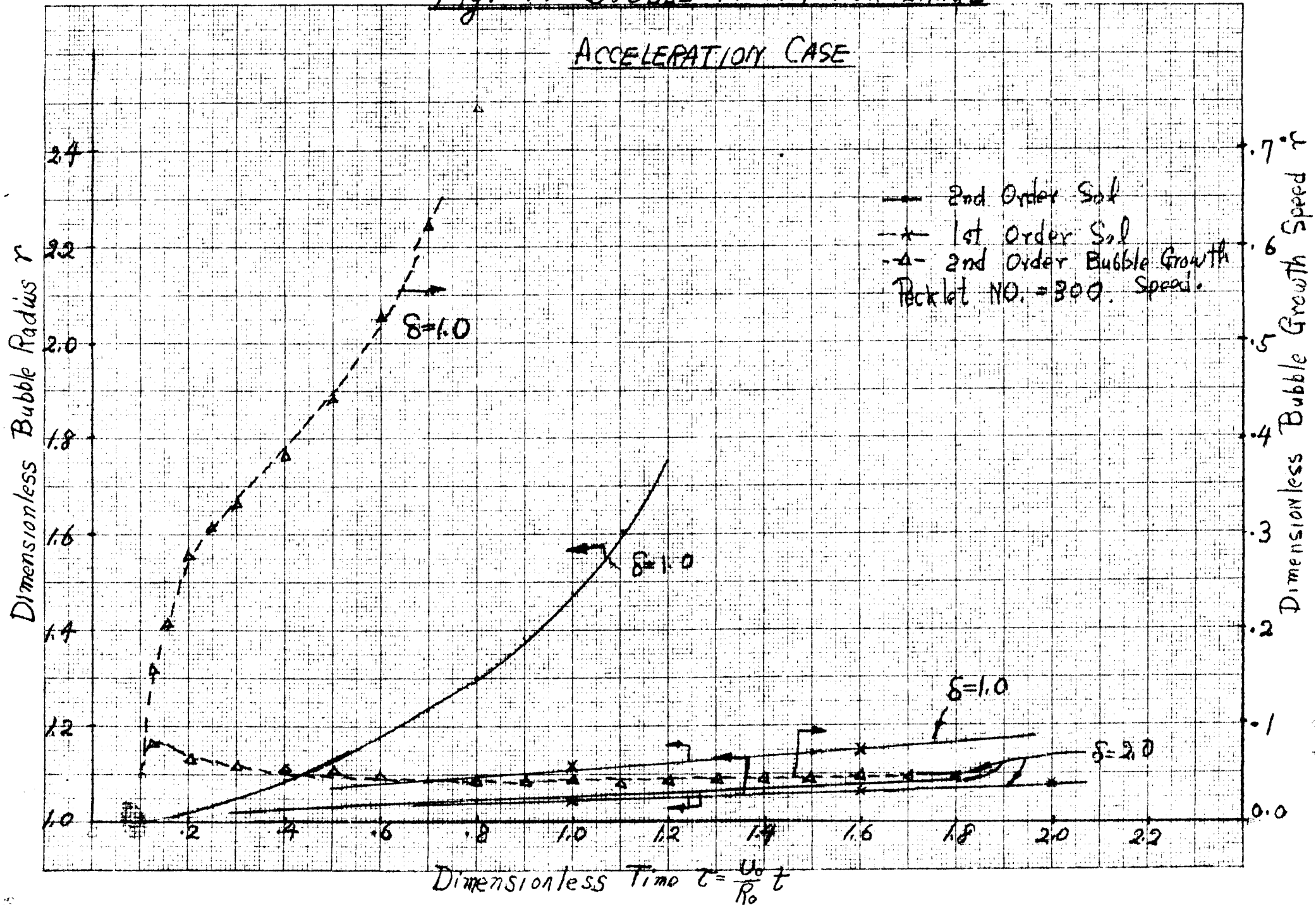


Fig. 24. BUBBLE GROWTH FOR LARGE

ACCELERATION CASE



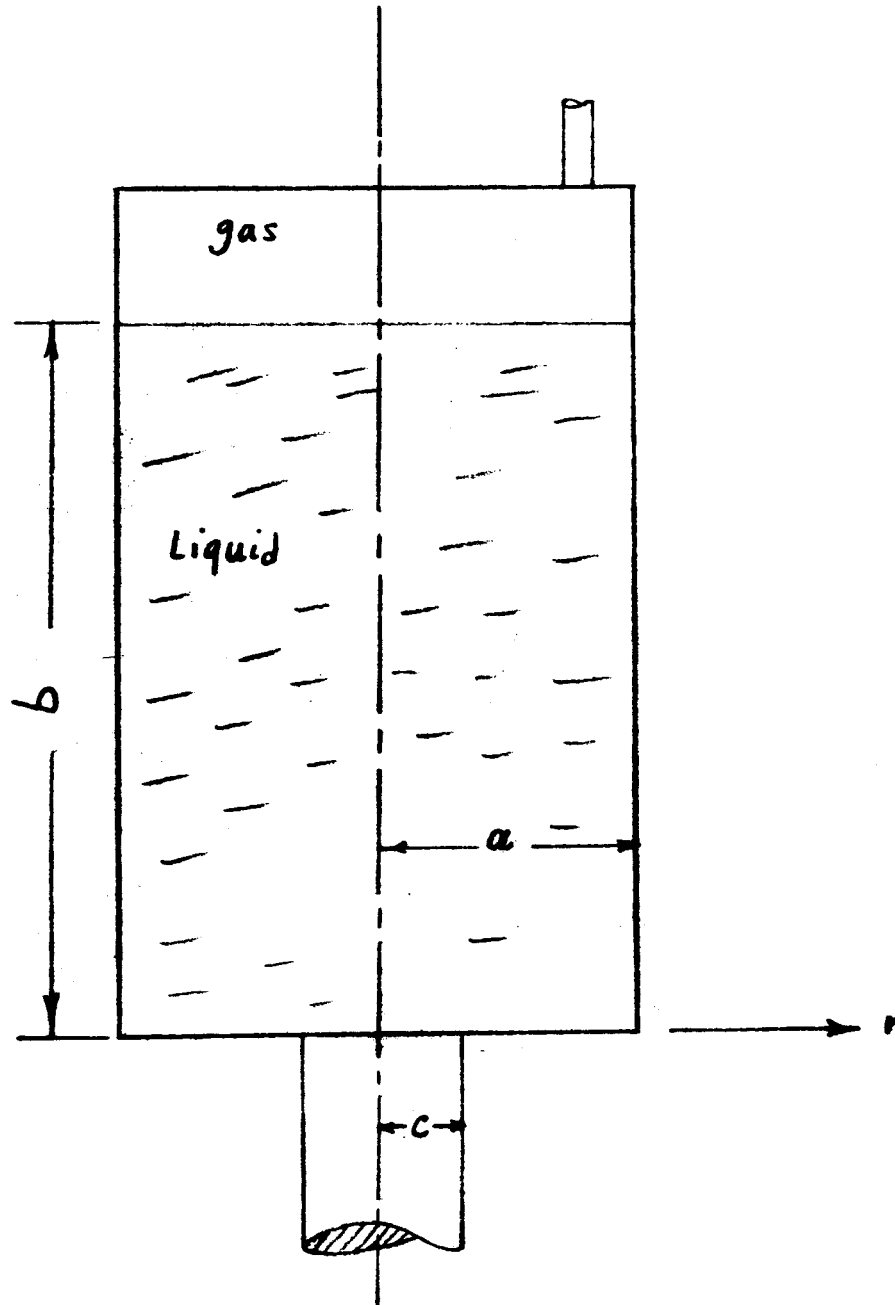
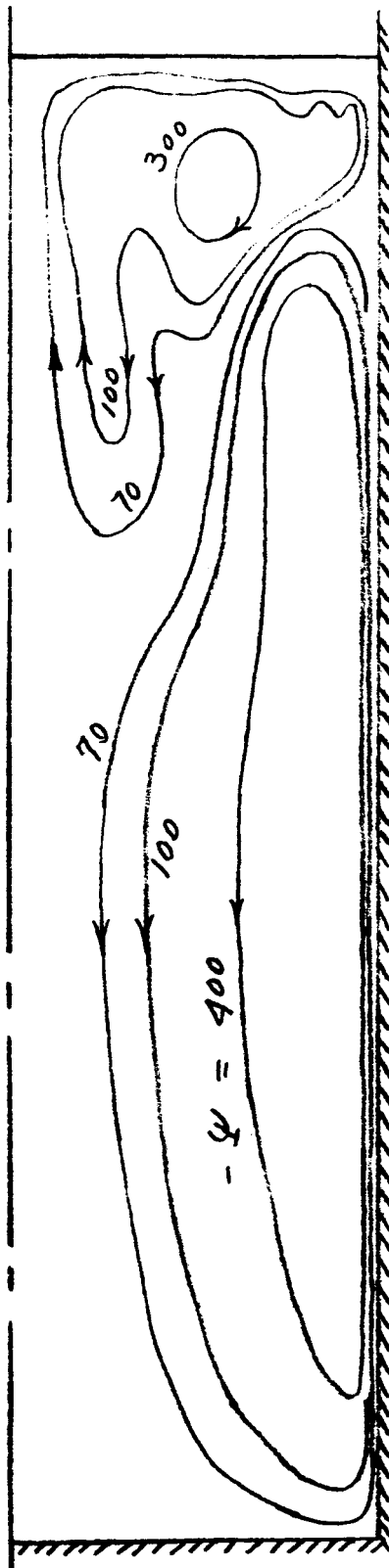


Figure 25. Coordinate system for cylindrical tank.



Flow Pattern

$(\psi/A)_w = 400$

$T_{surf.} = T_{sat.}$

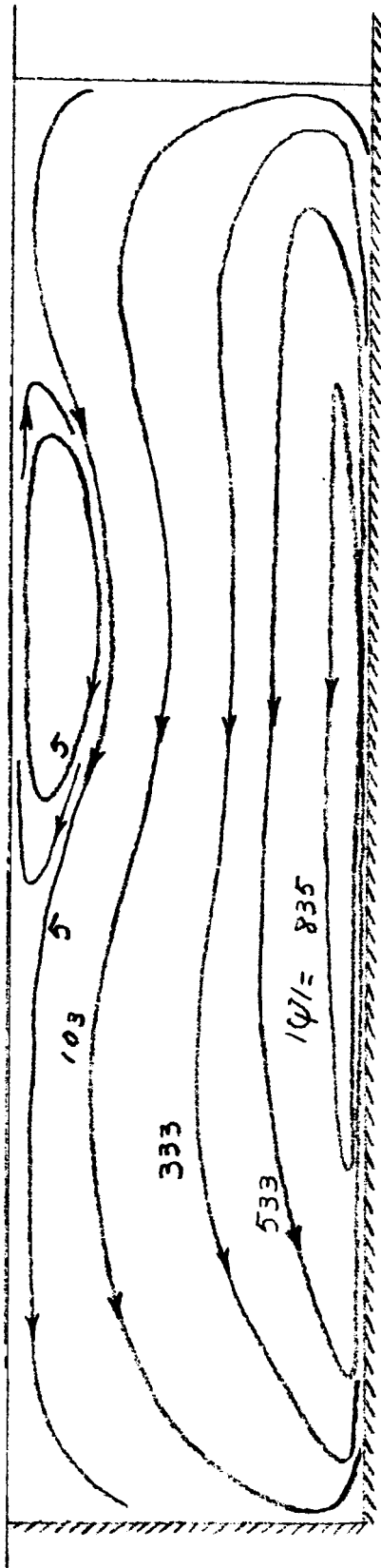
$\zeta = 1.57 \times 10^{-4}$

$= 11.4^\circ$

$R = 0.25$

$\frac{R}{H} = 0.25$

Figure 26. Transient flow pattern for cylindrical tank—small time.



Flow Pattern

$(\frac{\rho}{A})_w = 400$

$T_{SURF} = T_s$

$\bar{\epsilon} = .00042$

$= 30''$

$R = 0.25$

$\frac{R}{H} = 0.25$

Figure 27. Transient flow pattern for cylindrical tank—large time.